

Discovery and Structure-Based Optimization of Next Generation Reversible Methionine Aminopeptidase-2 (MetAP-2) Inhibitors

Timo Heinrich, Jeyaprakashnarayanan Seenisamy, Beatrix Blume, Jörg Bomke, Michel Calderini, Uwe Eckert, Manja Friese-Hamim, Rainer Kohl, Martin Lehmann, Birgitta Leuthner, Djordje Musil, Felix Rohdich, and Frank T. Zenke

J. Med. Chem., **Just Accepted Manuscript** • DOI: 10.1021/acs.jmedchem.9b00041 • Publication Date (Web): 02 Apr 2019

Downloaded from <http://pubs.acs.org> on April 3, 2019

Just Accepted

“Just Accepted” manuscripts have been peer-reviewed and accepted for publication. They are posted online prior to technical editing, formatting for publication and author proofing. The American Chemical Society provides “Just Accepted” as a service to the research community to expedite the dissemination of scientific material as soon as possible after acceptance. “Just Accepted” manuscripts appear in full in PDF format accompanied by an HTML abstract. “Just Accepted” manuscripts have been fully peer reviewed, but should not be considered the official version of record. They are citable by the Digital Object Identifier (DOI®). “Just Accepted” is an optional service offered to authors. Therefore, the “Just Accepted” Web site may not include all articles that will be published in the journal. After a manuscript is technically edited and formatted, it will be removed from the “Just Accepted” Web site and published as an ASAP article. Note that technical editing may introduce minor changes to the manuscript text and/or graphics which could affect content, and all legal disclaimers and ethical guidelines that apply to the journal pertain. ACS cannot be held responsible for errors or consequences arising from the use of information contained in these “Just Accepted” manuscripts.

Discovery and Structure-Based Optimization of Next Generation Reversible Methionine

Aminopeptidase-2 (MetAP-2) Inhibitors

Timo Heinrich,^{*1} Jeyaprakashnarayanan Seenisamy,² Beatrix Blume,¹ Jörg Bomke,¹ Michel Calderini,¹ Uwe Eckert,¹ Manja Friese-Hamim,¹ Rainer Kohl,¹ Martin Lehmann,¹ Birgitta Leuthner,¹ Djordje Musil,¹ Felix Rohdich,¹ Frank T. Zenke¹

¹Merck Healthcare, Merck KGaA, Frankfurter Str. 250, 64293 Darmstadt, Germany; ²Syngene International Ltd., Biocon Park, Plot 2&3, Bommasandra-Jigani Link Road, Bangalore 560 099, India

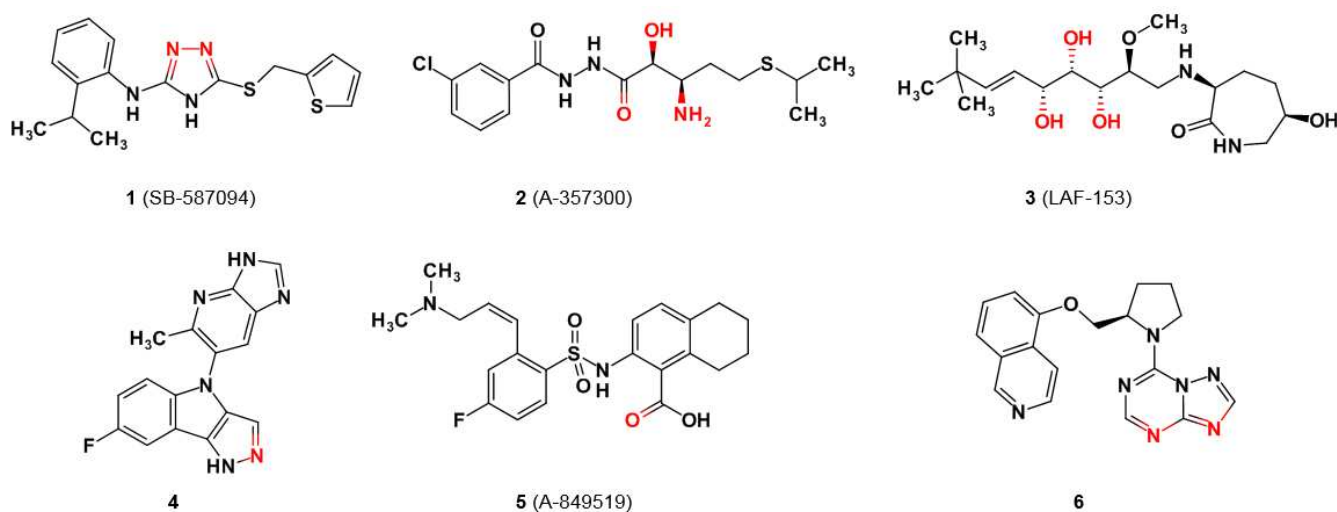
Abstract

Co- and post-translational processing are crucial maturation steps to generate functional proteins. MetAP-2 plays an important role in this process and inhibition of its proteolytic activity has been shown to be important for angiogenesis and tumor growth suggesting that small molecule inhibitors of MetAP-2 may be promising options for the treatment of cancer. This work describes the discovery and structure-based hit optimization of a novel MetAP-2 inhibitory scaffold. Of critical importance, a cyclic tartronic diamide coordinates the MetAP-2 metal ion in the active site while additional side chains of the molecule were designed to occupy the lipophilic methionine side chain recognition pocket as well as the shallow cavity at the opening of the active site. The racemic screening hit from a HTS campaign **11a** was discovered with an enzymatic IC₅₀ of 150 nM. The re-synthesized eutomer confirmed this activity and inhibited HUVEC proliferation with an IC₅₀ of 1.9 μM. Its structural analysis revealed a sophisticated interaction pattern of polar and lipophilic contacts that were used to improve cellular potency to an IC₅₀ of 15 nM. In parallel, the molecular properties were optimized on plasma exposure and anti-tumor efficacy which led to the identification of advanced lead **21**.

Introduction

Methionine aminopeptidase-2 (MetAP-2) is responsible for cleaving N-terminal methionine residues of proteins which is an important step of protein maturation during protein synthesis. Inhibition of MetAP-2 effectively impairs angiogenesis and tumor growth making it an attractive target for anticancer

1
2
3
4
5
6 therapy.^{1,2} Recently, analogs of the natural product MetAP-2 inhibitor fumagillin have been evaluated in
7
8 clinical trials in oncology and obesity.³ These fumagillin analogs are known to covalently bind MetAP-2
9
10 and have to be administered subcutaneously or intravenously and, thus, have limited therapeutic utility.⁴
11
12 One fumagillin analog, TNP-470, was extensively evaluated in clinical trials but was finally discontinued,
13
14 probably due to unfavorable pharmacokinetics as well as neurotoxicological side effects which were
15
16 considered to be drug-related.⁵ However, it is conceivable that non-covalent, non-fumagillin small
17
18 molecule inhibitors of MetAP-2 may have different tolerability in a clinical setting. The chemical diversity
19
20 of small molecule MetAP-2 inhibitors described until now is quite broad and X-ray crystallography has
21
22 helped to identify critical aspects how MetAP-2 inhibitors bind in the proteolytic cleft and to the
23
24 catalytically important metal ions. Figure 1 depicts the ligands for which the binding mode has been
25
26 identified by X-ray structure analyses. The center(s) reported to coordinate the metal ion(s) are marked
27
28 in red (distance <3 Å).
29
30



50
51
52
53
54
55
56
57
58
59
60

Figure 1: reversible MetAP-2 inhibitors. X-Ray structure analyses published. Metal cofactor binding atoms marked in red; PDB codes added: 1 (SB-587094) 2OAZ; 2 (A-357300) 1R58; 3 (LAF-153) 1QZY; 4 - 5JFR; 5 (A-849519) 1YW9; 6 - 5LYX.

This collection shows that one to three heteroatoms can bind to the metal ions⁶ in the active site of MetAP-2, and the arrangement of either oxygen or nitrogen or both in one scaffold is accomplished with

1
2
3
4
5
6 diverse chemical matter. For the triazole **1** (SB-587094) it was shown that both of the adjacent nitrogens
7
8 are necessary to achieve single digit nanomolar biochemical inhibition constant (K_i) values with cobalt as
9
10 co-factor. Methylation of either nitrogen spoils affinity significantly.⁷ The 2-hydroxy-3-aminoamide
11
12 grouping of the bestatin⁸ like **2** (A-357300) interacts with the active site Mn^{2+} metal ions,⁶ and the 2-
13
14 hydroxy substituent is bridging between the ions. The thioether-containing sidechain largely fills the
15
16 adjacent hydrophobic site, while the 3-chlorophenyl aromatic group lies face to face with the His339
17
18 imidazole. An IC_{50} value of 110 nM in the enzyme assay was reported for this inhibitor.⁹ The t-butyl group
19
20 of bengamide analog **3** (LAF-153) extends into the innermost portion of the cleft, whereas the lactam
21
22 ring is coordinated in the shallow pocket at the surface of the enzyme. All three hydroxyl groups
23
24 coordinate to the two cobalt ions in the published structure.^{10, 11, 12} In contrast to these very flexible open
25
26 chain MetAP-2 inhibitors compound **4** from Takeda is much more rigid as two heterocyclic moieties are
27
28 linked via just one rotatable bond. One nitrogen of the pyrazole interacts directly with one metal ion
29
30 while the other protonated nitrogen builds up a water mediated interaction with the other manganese
31
32 ion. The phenyl ring of the core is well situated to make an edge-to-face interaction with the aromatic
33
34 side chain of Tyr444. The 7-fluoro substituent protrudes into the lipophilic pocket occupied by the
35
36 thioether of the endogenous substrates, making the ligand very shape complementary with the target.
37
38 The aza-benzimidazole substituent at the N-4 position points into a hydrophobic space between Tyr444-
39
40 and His339-side chain. This compound was reported with a pIC_{50} of 8.3.¹³ The carboxylate **5** (A-849519)
41
42 was published with two digit nanomolar IC_{50} in enzyme inhibition assay. Only one oxygen of the acid
43
44 function is in direct contact to one of the manganese ions but the other heteroatom, like in case of the
45
46 pyrazole **1**, is binding to a water molecule positioned over both metal ions.¹⁴ For the substituted triazolo-
47
48 triazine **6** as well as for analogous derivatized purines it was demonstrated that both southern nitrogens
49
50 are in direct contact to manganese ions, even though the assignment changes (180° flip).¹⁵ In addition to
51
52 these published MetAP-2 co-structures of reversible ligands, further literature known inhibitors were
53
54
55
56
57
58
59
60

synthesized and crystallized to extend the structural knowledge of reversible MetAP-2 inhibitors (Figure 2).

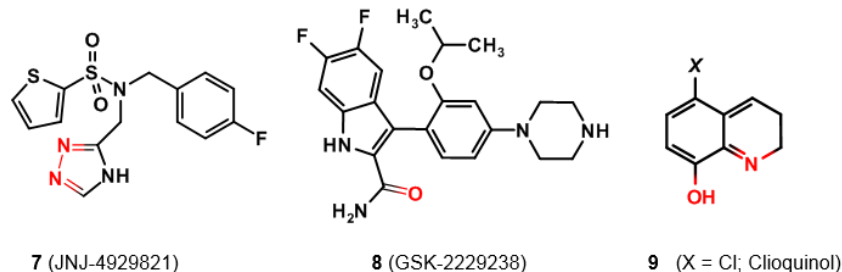
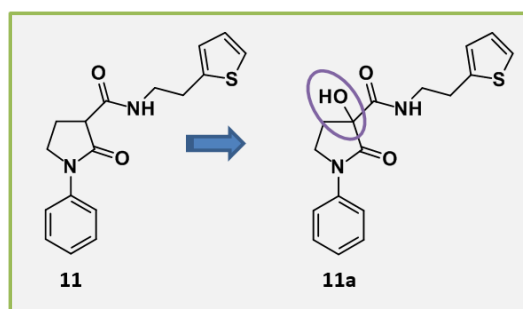


Figure 2: reversible MetAP-2 inhibitors. Synthesis and structural analyses performed in house. PDB codes added: 7 (JNJ-4929821) 6QEJ; 8 (GSK-2229238) 6QEI, 9 (X = Cl; Clioquinol) 6QEH.

As **1**, **7** (JNJ-4929821)¹⁶ contains a 4H-[1,2,4]-triazole as metal coordinating heterocycle, but **8** (GSK-2229238)¹⁷ is the first carboxamide described as MetAP-2 inhibitor. The terminal triazole from **7** superimposes quite well with the di-substituted derivative **1**, supporting the hypothesis that the adjacent nitrogens are necessary for MetAP-2 binding. The carboxamide in **8** is substantially differently oriented than the carboxylate of **5**. Only the oxygen of the amide function is binding to one metal ion but the nitrogen is not involved in any water mediated hydrogen bond network. It is in 3.35 Å distance to the imidazole of His331. Clioquinol **9** and the nitro analog nitroxoline **10** (X = NO₂; APL-1202) are known antibiotics for the treatment of urinary tract infections and are described to inhibit MetAP-2 activity.^{18,19} Nitroxoline **10** is reported with an IC₅₀ value of 55 nM in the enzymatic MetAP-2 inhibition assay and interferes in HUVEC (human umbilical vein endothelial cells) proliferation, but only with micromolar potency (IC₅₀: 1.9 μM). In the context of repurposing activities clinical investigations are on-going to develop **10** for the treatment of invasive bladder cancer.^{20,21} The hydroxy-quinoline coordinates both metal ions with the oxygen binding to the more buried ion in 2 Å, and the quinoline nitrogen to the second ion in 2.51 Å distance as found for **9**. The chlorine is directed into the lipophilic substrate recognition pocket and is in vdW contacts to Ala414 (4.32 Å), His231 (3.82 Å) and His382 (4.18). During inhouse work with purine based MetAP-2 inhibitors it was not possible to optimize biochemical activity

1
2
3
4
5
6 of compounds based on purine-and related scaffolds like **6** to a low nanomolar level. More important,
7
8 the relatively weak enzymatic potency did not translate into favorable HUVEC proliferation inhibition in a
9
10 consistent manner, considered to be required to elicit significant *in vivo* efficacy (tumor growth
11
12 inhibition).¹⁵ Accordingly, focus was switched to another HTS hit series comprised during a screening
13
14 campaign not taken into account during first result evaluations. This hit matter was re-considered
15
16 because of missing compelling alternatives. Insufficient purity was the reason for initial de-prioritization,
17
18 even though sub-micromolar activity was measured (IC₅₀ of 150 nM for the most potent derivative).
19
20 Accordingly, a more detailed analysis of the series was conducted, and it became obvious that these hits
21
22 relinquished a consistent pattern responsible for their failure in post-HTS control. In all cases, the
23
24 detected molecular mass was 16 units larger than the mass for the registered structure. Oxidation was
25
26 responsible for this deviation between expected and observed molecular mass, and NMR analysis
27
28 revealed the position of the oxidized center (Figure 3).
29
30



47
48
49
50
51
52
53
54
55
56
57
58
59
60

Figure 3: The stored α -amidated pyrrolidinone **11 was oxidized to the cyclic tartronic di-amide **11a** under storage in DMSO over approximately 2 years.**

C α of the pyrrolidinone in **11** is substituted with an amide residue, activating this carbon for oxidation. The screening sample had been stored for 2 years as DMSO stock solution in a sealed tube at -20°C. Obviously, these conditions were not sufficient to prevent quantitative oxidation. Registration analytics of the compound confirmed the envisioned original structure of **11**, and a newly synthesized batch did not show any activity in the biochemical assay. The dedicated synthesized compound **11a** delivered an IC₅₀ of 57 nM confirming the initial screening result. Attempts to mimic the oxidation of **11** to **11a** during

storage by stirring the reduced precursor **11** in DMSO at higher temperature for a couple of days were not successful (no oxidation could be detected). The compound had been included in many HTS initiatives shortly before the MetAP-2 screen and afterwards, but never showed any activity. This suggested a very high overall target selectivity. Thus, persistence and serendipity helped to identify the starting point for the herein outlined optimization.

The structural analysis of the hit **11a** challenges virtually every atom of the ligand. Our systematic optimization was graded by pragmatic considerations and scaffold dissections (Figure 4).

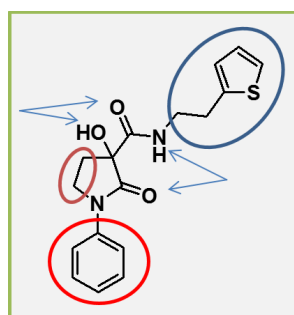
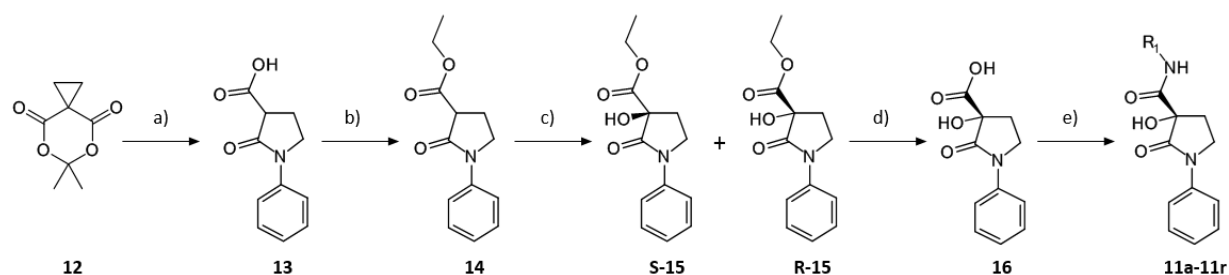


Figure 4: Screening hit *rac*-11a with indications of different parts of the molecule. The first optimization cycle focused on the amide residue highlighted by a blue circle; second improvement round considered the N-lactam residue marked with a red circle. The investigation of lactam size and additional substitutions (brown circle) as well as the heteroatoms (indicated with arrows) are not discussed here.

Chemistry

All compounds described herein belong to the same pyrrolidinone class but were prepared via alternative approaches, depending on the optimization purpose. The preparation of optimized amides followed the procedure out-lined in Scheme 1.

Scheme 1: Synthetic approach to optimize amide residue R_1 . Derivatives from tables 1 and 2.^a

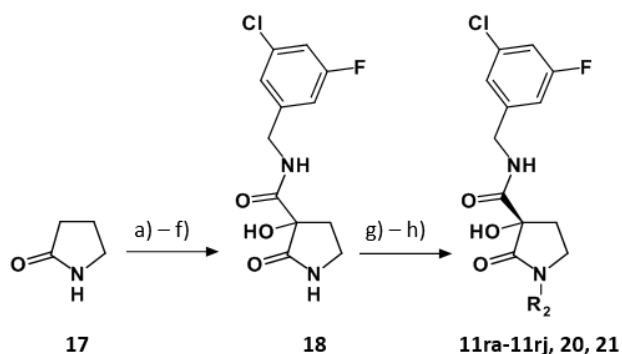


^aReagents and conditions: a) ACN, aniline, 60°C, 12h, 85%; b) EtOH, SOCl₂, 0°C – reflux, 4h, N₂; 92% c) CeCl₃·(H₂O)₇, iPrOH, O₂, 12h, RT; Chiralpak AD-H; d) LiOH, THF/H₂O, 4h, RT; 84% e) R₁-NH₂, EDCI, HOBT, 160°C, MW, 20 min 40 – 80%.

This approach started with the reaction of cyclopropyl Meldrum's acid **12** with aniline to give N-Phenyl-pyrrolidinone-3-carboxylic acid **13** which was then transferred into the corresponding ethyl ester **14** with thionyl chloride in ethanol. C3 oxidation of the pyrrolidinone-3-carboxylate **14** was achieved with cerium chloride in ethanol. C3 oxidation of the pyrrolidinone-3-carboxylate **14** was achieved with cerium chloride in isopropanol. The functionalized pyrrolidinone was separated into the enantiomers **S-15** and **R-15** via chiral chromatography and the desired enantiomer **R-15** was saponified with lithium hydroxide in a THF/water mixture of 3:1 to the corresponding acid **16**. The hydroxy-acid **16** was coupled under standard conditions with amines to the amides **11a-11r**.

The second optimization round focused on the lactam nitrogen substituent. In this context an alternative synthesis was established. In the initial approach aniline was reacted with Meldrum's acid, introducing the lactam substituent in the first reaction. However, this procedure was considered to be unpractical for an optimization of the lactam nitrogen residue which should be added in the last step of the synthesis. Accordingly, the sequence outlined in Scheme 2 using the identified 3-chloro-5-fluoro-benzylamine as suitable residue R₁ was established.

Scheme 2: Synthetic approach to optimize lactam residue R₂. Derivatives from table 3^a



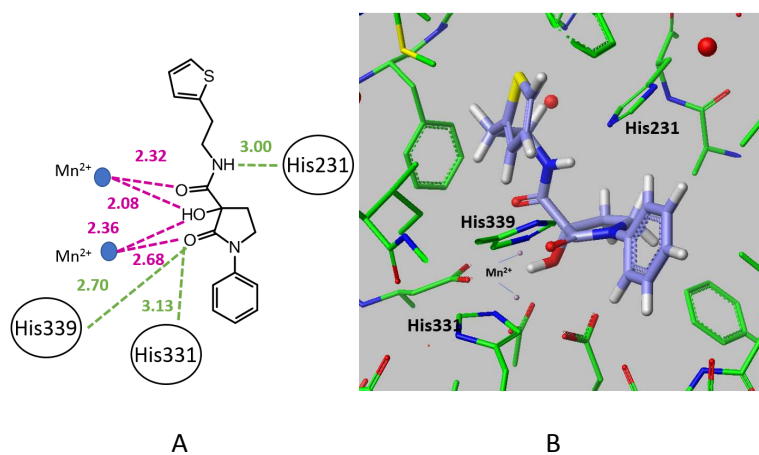
^aReagents and Conditions: a) BOC₂O, DMAP, ACN, 3h, RT, 70%; b) benzyl chloroformate, LiHMDS, THF, 2h, -78°C – RT, 42%; c) Pd/charcoal, methanol, H₂, 2 bar, 2h RT, 86%; d) 3-F, 5-Cl benzylamine, T3P, TEA, DCM, 5h, 0°C – RT, 86%; e) TFA, DCM, 3h, 0°C, 90%; f) MMPP, DMF, 4h, 70°C, 37%; g) R₂-halide, K₂CO₃, CuI, N,N'-diethyl-ethane-1,2-diamine, dioxane, 2h, 140°C, MW; h) Chiralpak AD-H.

1
2
3
4
5
6 Commercially available pyrrolidinone **17** was first BOC protected. Different options were worked out to
7
8 introduce the carboxylic moiety in position 3. Reproducible results were obtained by deprotonation with
9
10 lithium bis(trimethylsilyl)amide (LiHMDS) and quenching with benzyl chloroformate. Hydrogenation of
11
12 the benzyl ester, subsequent amidation of the acid with 3-fluoro, 5-chloro benzylamine in the presence
13
14 of 2,4,6-Tripropyl-[1,3,5,2,4,6]trioxatriphosphinane 2,4,6-trioxide (T3P) and deprotection of the lactam
15
16 nitrogen proved to be necessary to oxidize the chiral carbon with magnesium monoperoxyphthalate
17
18 hexahydrate (MMPP) to give the key intermediate **18**. Established Buchwald conditions were used to
19
20 arylate the lactam nitrogen. The racemic products from this approach were separated into the
21
22 enantiomers via chiral chromatography giving the final products **11ra-11rj**, **19** and **20**.

23 24 25 Results and Discussion

26
27 For the determination of potency of MetAP2 inhibitors an enzyme-coupled assay to measure the
28
29 proteolysis of a tripeptide substrate (Met-Ala-Ser) was established. Recombinant purified His-TEV-
30
31 MetAP-2 (AA2-478) with manganese as a co-factor was used.⁶ Proliferation of HUVEC primary
32
33 endothelial cells was applied as mechanistical assay to assess compound potency in the cellular
34
35 environment.²²

36
37
38 Crystallization of the human MetAP-2 protein fragment, comprising amino acid residues 108 – 478 had
39
40 been established during earlier work¹⁵ so this tool could be used to understand the binding mode of **11a**
41
42 (Figure 5 & Figure 6):
43
44



1
2
3
4
5
6 **Figure 5: X-ray structure analysis of 11a in MetAP-2; A: 2D plot to show relevant polar interactions,**
7 **indicated with dashed lines, oxygen-manganese contacts in purple, heteroatom-His^{imidazole} in green,**
8 **distances are given in Ångstrom; B: Conformation of 11a in the active site; interacting imidazoles of**
9 **His331 and His339 and the manganese ions are pointed out (PDB: 6QEG).**
10

11
12 The schematic 2D plot of Figure 5A depicts the polar interactions of **11a** with the protein. The oxygen at
13
14 C α of the tartonic di-amide coordinates the two manganese ions in the active site of MetAP-2. The
15
16 distance to the first, less buried ion is 2.36 Å and to the second ion, which is deeper located in the
17
18 pocket, 2.08 Å. The lactam oxygen is also in close contact to the first metal ion with 2.68 Å, and the
19
20 amide oxygen binds to the second ion with a distance of 2.32 Å. The three oxygens of the α -hydroxy-
21
22 malonic di-amide form a unique metal binding element that is unprecedented for MetAP-2 inhibitors.²³
23
24 The binding of compound **11a** to MetAP-2 is characterized by additional polar interactions. In addition to
25
26 its metal coordination, the lactam oxygen interacts with the protons from His339-imidazole (2.70 Å) and
27
28 His331-imidazole (3.31 Å). The amide NH is in H-bond distance to His231 side chain (3 Å). The high
29
30 electron density of this imidazole is documented by its nucleophilic attack on the epoxide of covalently
31
32 binding fumagillin type natural products and derivatives.²⁴ Figure 5B shows the active site of MetAP-2
33
34 with **11a**. The lactam ring is the planar template of this MetAP-2 inhibitor class from which the residues
35
36 are positioned for relevant protein interaction. The N-phenyl ring of compound **11a** covers the entrance
37
38 to the active site and is rotated by 62° out of the lactam plane. The hydroxy function is pointing
39
40 downwards and is coordinated to both manganese ions in the active site. The amide residue is pointing
41
42 up-wards and is allowing the thiophene-ethyl residue to orient itself in the substrate recognition area of
43
44 MetAP-2.
45
46
47
48
49
50
51
52
53
54
55
56
57
58
59
60

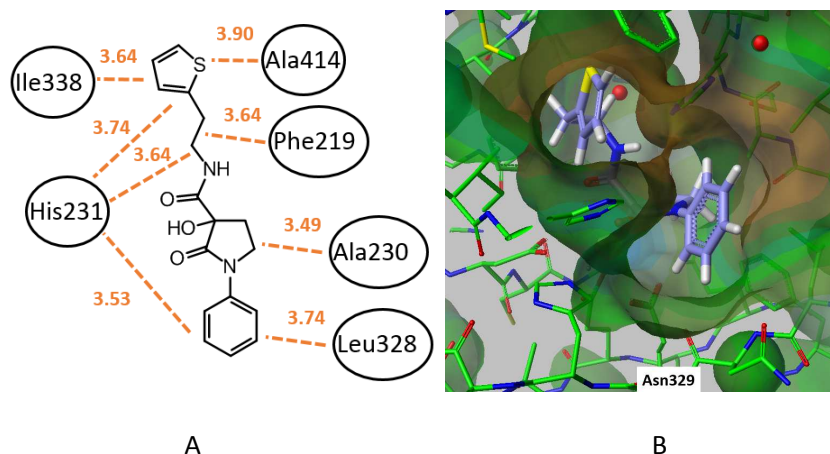


Figure 6: X-ray structure analysis of 11a in MetAP-2: A: 2D plot to show relevant lipophilic interactions, indicated with dashed lines, distances are given in Ångstrom; B: identical view on the conformation of 11a in the active site as in figure 3 B; the lipophilic trait of the protein surface is color coded. Brown indicates a lipophilic surface, green a polar one (PDB: 6QEG).

Figure 6 A illustrates the van der Waals (vdW) distances of the ligand **11a** to the amino acid side chains in the active site. The thiophene is located in the nonpolar area that accommodates the methionine side chain upon hydrolysis of natural substrates. Not only the side chains of Ala414 and Ile338 are in vdW contacts with the thiophen but also the imidazole of His231. In addition, this imidazole has also lipophilic interactions with the ethyl bridge between the amide nitrogen and the thiophene. These observations of polar and lipophilic interactions of the imidazole heterocycle of His231 demonstrate that this is the most crucial amino acid for inhibitor recognition. The lactam N-phenyl ring of **11a** faces an amphiphilic surrounding. The properties of the bottom part of the active site (as oriented in Figure 6B) are driven by the backbone -oxygen and -nitrogen of Asn329. These heteroatoms are responsible for constituting a polar region whereas the protein surface in the upper-right region is lipophilic due to the domination of the methyl and iso-butyl side chains of Ala230, Leu447 and Leu328 (not explicitly indicated in Figure 6B). The protein surface around the unsubstituted carbons C4 and C5 of the lactam ring of **11a** is amphiphilic, too. Carbon C5 is in vdW contacts to the side chains of Ala230 (3.49 Å) and Phe399 (3.9 Å). Carbon C4 is pointing towards a polar cavity that occupies two crystal water molecules (not shown in Figure 6) and this carbon is virtually without any measurable interaction.

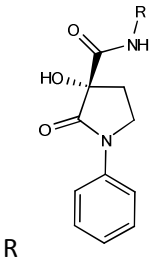
The structural analysis indicates that the *S*-enantiomer (*S*-**11a**) is bound to the protein. Accordingly, *rac*-**11a** was separated into the enantiomers via chiral chromatography on a SFC device. Both enantiomers were assessed in the enzyme inhibition assay and the eutomer was found with an IC₅₀ value of 0.053 μM. Our structural analyses (NMR, X-ray) indicated that the stereochemistry of the active isomer is confirmed to have *S* configuration at the chiral carbon (Table 1). **R-11a** inhibits MetAP-2 with an IC₅₀ of 13 μM, which is >200 times less active than the *S* enantiomer. During the optimization process we continued to separate enantiomers via chiral chromatography from racemic syntheses but for production of larger compound quantities we established an asymmetric synthesis route for most efficient drug production.²⁵

Amide Chain length and substitution

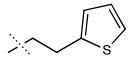
The easily adjustable and deeply buried amide residue was considered at first during optimization, as a strong impact on potency was anticipated. The residue attached to the lactam nitrogen was deemed to play an important role for binding affinity, too. Though not as submerged as the amide substituent, the X-ray analysis revealed contacts for the phenyl ring with the protein surface as insinuated above (Figure 5 and Figure 6B). This awareness suggested a dedicated optimization of the lactam N-substituent during second approach.

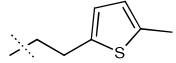
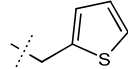
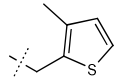
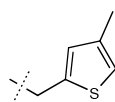
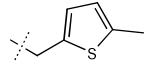
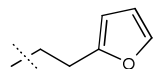
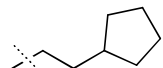
The expansion of the thiophene with a methyl group beside the sulfur (**11b**) should fill in the pocket superior to the unsubstituted thiophene of **11a**. Apparently, the contrary is the case as the methylated analog **11b** of the original hit **11a** is three times less active (Table 1).

Table 1: initial SAR of amide residue^a

MSC		Enzyme IC ₅₀ [μM]	HUVEC proliferation IC ₅₀ [μM]
<i>rac</i> - 11a		0.057 +/- 0.08	NT ^b

1
2
3
4
5
6
7
8
9
10
11
12
13
14
15
16
17
18
19
20
21
22
23
24
25
26
27
28
29
30
31
32
33
34
35
36
37
38
39
40
41
42
43
44
45
46
47
48
49
50
51
52
53
54
55
56
57
58
59
60

S-11a		0.050 +/- 0.006	1.9 +/- 0.93
R-11a		17 +/- 2.1	ND ^c

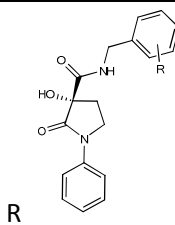
11b		0.22 +/- 0.07	2.9 +/- 0.21
11c		0.38 +/- 0.05	18 +/- 4.2
11d		0.41 +/- 0.09	18 +/- 1.3
11e		0.74 +/- 0.33	5.2 +/- 2.7
11f		0.48 +/- 0.18	15 +/- 1.4
11g		0.17 +/- 0.06	9.7 +/- 5.2
11h		0.14 +/- 0.03	2.5 +/- 0.57

^avalues are mean of three repetitions; ^bNT: not tested; ^cND: no IC₅₀ detectable

Comparison of **11a** with a published structure of methionine in MetAP-2 (PDB: 1wkm) revealed differences in the positions of the sulfur atoms of the thiophen in **11a** and of the thioether from methionine side chain of about 3 Å (Supplement Information, Figure S1). It was anticipated that shortening the ethyl linker between the amide nitrogen and the thiophene should allow for better substrate mimicking and pocket occupancy. The truncated linker in **11c** was less potent than the methylated hit-derivative **11b**. Systematic methylation of the thiophene-carbons either confirmed (**11d**, **11f**) or even decreased activity (**11e**). Reduction of thiophene ring size by introduction of a furan resulted in a three-fold less potent compound (**11g**) compared to the screening hit. Further five membered rings with up to three heteroatoms and an array of substituents were investigated but for none the activity

could be optimized. Hence, these derivatives are not discussed in detail here. The saturated amide residue of **11h** was by factor of three less active as **11a** and does not suggest that reduction of aryl load is beneficial for increased potency. This observation was confirmed by additional analogs which are not out-lined explicitly. Neither five membered aromatic nor saturated linear nor cyclic moieties allowed a potency increase and consequently larger residues were investigated (table 2). The unsubstituted benzyl derivative **11i** was also not a very promising residue as it showed an IC₅₀ of 440 nM what was factor eight less potent than the screening hit **11a**. Systematic permutation of one chlorine atom on the benzyl ring proved that ortho (**11j**) and meta (**11k**) substitution delivered more potent compounds than para substitution, with an IC₅₀ of 5.3 μM for the latter and sub-micromolar IC₅₀ for the other two. Accordingly, further investigations focused on the ortho and meta positions. Also, with fluorine as substituent the meta (**11n**) substitution showed slightly higher potency than the ortho (**11m**) position. The activity in the HUVEC proliferation assay was also better for the ortho substituted isomers compared to their meta analogs (**11j** vs **11k** and **11m** vs **11n**).

Table 2: second SAR of amide residue^a

No		Enzyme IC ₅₀ [μM]	HUVEC proliferation IC ₅₀ [μM]
11i	H	0.44 +/- 0.04	8.9 +/- 3
11j	2-Cl	0.27 +/- 0.04	18 +/- 5.9
11k	3-Cl	0.24 +/- 0.01	1.5 +/- 0.42
11l	4-Cl	5.3 +/- 1.2	ND ^b
11m	2-F	0.28 +/- 0.04	5.2 +/- 0.92
11n	3-F	0.14 +/- 0.001	1.6 +/- 0.071

11o	3-Me	0.55 +/- 0.04	4.0 +/- 2.8
11p	3,5-Cl ₂	0.06 +/- 0.02	0.35 +/- 0.14
11q	3,5-F ₂	0.08 +/- 0.01	0.25 +/- 0.081
11r	3-Cl, 5-F	0.06 +/- 0.006	0.1 +/- 0.085

^avalues are mean of three repetitions; ^bND: no IC₅₀ detectable

It was expected that the fluorine substitution of the benzylic moiety should be favorable in terms of compound properties compared to aliphatic moieties. Nevertheless, the meta-methyl benzylamide **11o** was prepared as favorable lipophilic contacts had been anticipated. Surprisingly, **11o** had reduced biochemical and cellular activity compared to the meta-F derivative **11n**. This observation motivated the further analyses of halogen substitutions. The introduction of a second meta halogen improved biochemical activity. In the enzymatic testing the bis-chloro (**11p**) and bis-fluoro (**11q**) benzylamides proved to be as active as the fluoro, chloro mixed analog **11r**. This similarity was confirmed in the anti-proliferative activity in the HUVEC assay. All three bis-halogen substituted benzyl amides (**11p**, **11q**, **11r**) impaired HUVEC proliferation with a low three digit nanomolar IC₅₀.

The structural analysis of “stopover” **11r** from the first optimization cycle clearly demonstrates how both halogen substituents are involved in vdW interactions in the lipophilic pocket (Figure 7). The fluorine atom (brown) is pointing upwards and towards the protein surface. It is involved in lipophilic interactions with the methylene group of His382 (3.41 Å) and the methyl-side chain of Ala414 (3.22 Å). The chlorine atom (light green) is pointing down-wards to be in contact with the imidazole side chain of His339 (3.51 Å). In addition, this chlorine is sandwiched between the side chain of Ile338 (3.68 Å) and Tyr444 (3.50 Å).

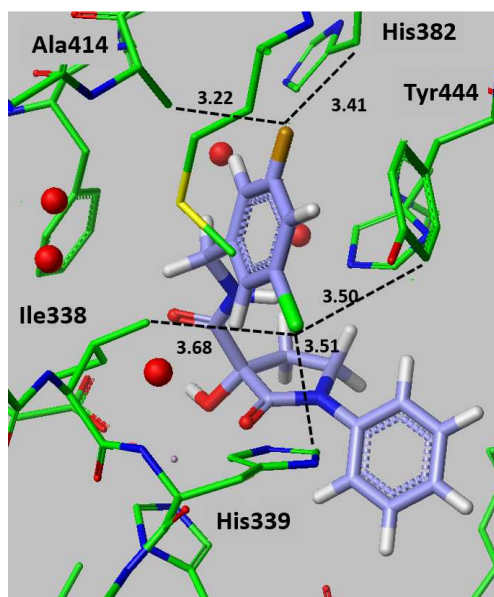


Figure 7: X-Ray structure analysis of the optimized amide residue in **11r. Depicted are only the distances of the halogens (F, top, brown; Cl, bottom, light green) on the benzamide to the amino acid side chains of MetAP-2 (**6QEF**).**

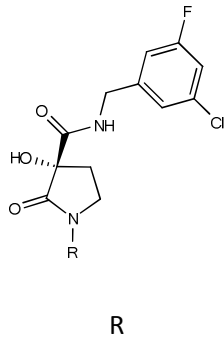
The oxygen atom of the alcohol function is coordinating the two manganese ions with distances of 2.08 Å and 2.19 Å, respectively, virtually identical to the position of this oxygen of the initial screening hit (distances of oxygen to metal ions are not explicitly shown in Figure 7).

Lactam residue

Benzamide **11r** was considered to be a good starting point for optimizing the lactam nitrogen substituent (Table 3). The unsubstituted building block **18** was still active and inhibited the isolated enzyme with an IC_{50} in the sub-micromolar range. Replacement of the proton with a methyl group (**19**) had virtually no effect on biochemical activity. The sub-micromolar activity of **18** and **19** in the enzyme assay clearly indicates the importance of tartronic-diamide motive for strong binding to MetAP-2.

Subsequent efforts focused on exploring the phenyl ring SAR through systematic evaluation of electron donating and electron withdrawing substituents. (Figure 5B).

Table 3: SAR of the N-lactam residue^a

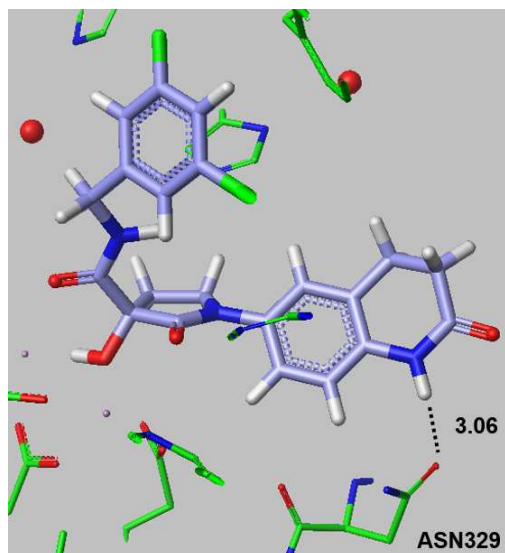
No		Enzyme IC ₅₀ [μ M]	HUVEC proliferation IC ₅₀ [μ M]
	R		
R-18	H	0.59 +/- 0.02	ND ^b
19	Me	0.7 +/- 0.007	ND ^b
11ra	2-Me-phenyl	0.54 +/- 0.17	17 +/- 2.8
11rb	3-Me-phenyl	0.09 +/- 0.001	0.3 +/- 0.12
11rc	4-Me-phenyl	0.09 +/- 0.02	0.24 +/- 0.078
11rd	2-CN-phenyl	0.86 +/- 0.31	29 +/- 1.3
11re	3-CN-phenyl	0.09 +/- 0.02	1.7 +/- 0.32
11rf	4-CN-phenyl	0.13 +/- 0.04	6.1 +/- 0.35
11rg	3-Acetamido-phenyl	0.08 +/- 0.04	0.28 +/- 0.095
11rh	4-Acetamido-phenyl	0.08 +/- 0.01	0.032 +/- 0.013
11ri	3-carbamoyl-phenyl	0.06 +/- 0.03	0.31 +/- 0.035
11rj	4-carbamoyl-phenyl	0.06 +/- 0.01	1.6 +/- 0.74
20	Oxindol-5-yl	0.05 +/- 0.01	0.17 +/- 0.07
21	2-Oxo-tetrahydro-quinolin-6-yl	0.074 +/- 0.03	0.015 +/- 0.01

^avalues are mean of three repetitions; ^bND: no IC₅₀ detectable

Even though all ortho-substituted derivatives (2-Me **11ra**, 2-CN **11rd**) were still sub-micromolar active in the enzyme assay, their cellular activity was hardly measurable. The meta and para methyl isomers **11rb** and **11rc** were equally potent having nanomolar IC₅₀ values in the biochemical and cellular assays. The polar cyano moiety was also not discriminating between the two positions, as the meta derivative **11re**

1
2
3
4
5
6 was as potent as the para isomer **11rf**. Cellular potency of these derivatives (**11ra – 11rf**) was in all cases
7
8 less favorable compared to the unsubstituted compound **11r**. The structural analysis of **11a** had
9
10 disclosed that the carboxamide side chain of Asn329 is responsible for a polar protein surface in the
11
12 bottom area depicted in Figure 5B. This observation served as rationale to provide a functionality
13
14 capable of H-bonding interaction to this amide group. The donor/acceptor orientation of the amide
15
16 residue of Asn329 should be flexible to allow for optimal interaction. Based on this prerequisite and the
17
18 anticipated distance an amide was considered to be a good H-bonding partner.²⁶ Both, para and meta
19
20 position phenyl carboxamides (**11ri, 11rj**) and acetamides (**11rg, 11rh**) were examined. While the enzyme
21
22 data for these derivatives was not significantly differentiated, the para-acetamide **11rh** led to the best
23
24 cellular response with an IC₅₀ in the two digit nanomolar range. Reduction of conformational flexibility of
25
26 the amide should minimize entropic penalties and should reduce rotational freedom contributing to
27
28 improved binding. Accordingly, the donor/acceptor- substitution pattern was captured in the oxindole **20**
29
30 and the more expanded analog **21**. The biochemical data looked quite the same for the open chain
31
32 (**11rh**) and both cyclic derivatives (**20, 21**) so that the working hypothesis to improve enzyme inhibition
33
34 had to be challenged. Surprisingly, a remarkable difference (factor of 10) was observed in the effect of **20**
35
36 vs **21** on HUVEC proliferation for these compounds. Efficient cellular growth impairment was achieved
37
38 with the 2-oxo-tetrahydro-quinolinylyl substitution of **21**. The reason for the better proliferation inhibition
39
40 can only be hypothesized but different binding kinetics might be responsible. The enzyme used for *in*
41
42 *vitro* enzyme inhibition is a recombinant His-tagged form and may behave differently than the native,
43
44 full-length MetAP-2 protein. Since a quite decent concentration of MetAP-2 enzyme had to be applied in
45
46 the biochemical assay the measured IC₅₀ values might already have reached the resolution for high
47
48 potency compounds. In addition, MetAP-2 associates with ribosomal subunits which may influence the
49
50 conformation of the protein and consequently, the potency of certain MetAP-2 inhibitors in cells. These
51
52 factors may account for some of the discrepancies observed between enzyme proliferation inhibition.
53
54
55
56
57
58
59
60

1
2
3
4
5
6 The optimized ligand was crystallized together with MetAP-2 and the structural examination of **21** is
7
8 depicted in Figure 8.
9



10
11
12
13
14
15
16
17
18
19
20
21
22
23
24
25
26
27
28 **Figure 8: X-ray structure analysis of 21 with focus on the additional polar interaction of the tetrahydro-**
29 **quinone-NH with the ASN329 side chain amide of MetAP-2 (6QED).**
30

31
32
33 In Figure 8 only the additional polar interaction between the lactam N-H with the oxygen of the Asn329
34 side chain amide is shown. The H-bond (3.06 Å) is probably contributing to the interaction of **21** with
35
36 MetAP-2.
37

38
39 For the covalent binding of irreversible inhibitors to the imidazole of His231 the nature of the metal ion
40 is of limited relevance. The ion might only function as Lewis acid, coordinating to the spiro-epoxide
41 oxygen to facilitate His231-imidazole attack.² All reversible ligands coordinate the metal ion co-factor.
42
43 Accordingly, identification of physiological metal cofactors for MetAP-2 is critical because literature
44 known inhibitors like A-310840 (3-[[[(naphthalen-2-yl)methyl]sulfonyl]-4H-1,2,4-triazole]) differentiate this
45 enzyme with different metal cofactors with potencies varying up to 1000-fold. *In vitro* investigations of
46 eight different metal ions on purified recombinant human MetAP-2 demonstrated that manganese, as
47 well as cobalt, maximally stimulate MetAP-2 activity indicating that either manganese or cobalt might be
48 the MetAP-2 cofactor *in vivo*.⁶ As such, compound **21** was evaluated in the enzyme assay with both
49
50
51
52
53
54
55
56
57
58
59
60

manganese and cobalt to determine if the hydroxy-malonic motif discriminates between the two metals.

Derivative **21** was found to be similarly active under cobalt and manganese assay conditions: $IC_{50} = 160$ nM vs 74 nM. Like other compounds from this new MetAP-2 binding class the development candidate is not active in the MetAP-1 enzyme assay.

The pK_a^{27} of **21** was determined to be around 11 and the $\log D^{28}$ at pH 7.4 is 2, explaining the good solubility profile in bio-relevant media (FaSSiF: 158 $\mu\text{g}/\text{ml}$; FeSSiF: 334 $\mu\text{g}/\text{ml}$). A favorable molecular weight of 431 Da and the tPSA of 99 contribute to good passive permeability and acceptable efflux in the Caco-2 assay ($a>b$: 16 $1E-6$ cm/s; ER: 5). The metabolic stability in liver microsomes from mouse and human was <10 $\mu\text{l}/\text{min}/\text{mg}$ protein qualifying the compound for further *in vivo* PK profiling. After iv dosing in mice, the compound showed favorable PK characteristics, i.e. clearance (CL), volume of distribution (Vss) and half-life ($t^{1/2}$) were determined to be 0.18 L/h/kg, 0.78 L/kg and 3 h, respectively. The oral bioavailability was 35% at 0.5 mg/kg and increased to $\sim 100\%$ at 50 mg/kg suggesting the saturation of a clearance mechanism (Figure 9). The favorable potency and PK data of **21** prompted us to investigate its tumor growth inhibition potential *in vivo*.

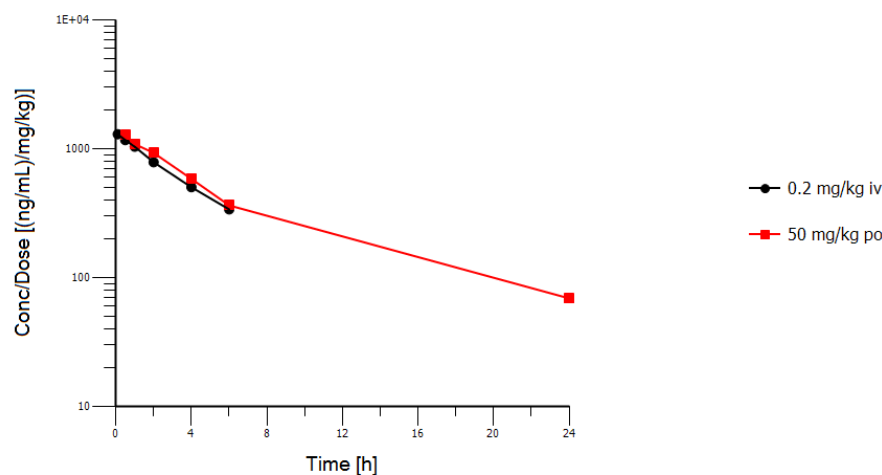


Figure 9: Dose-normalized plasma concentrations of 21 after 0.2 mg/kg iv and 50 mg/kg po dosing

For investigating *in vivo* efficacy of **21** the human glioblastoma U87-MG model was used. The tumor cells were subcutaneously injected in nude mice. Once tumors were established with a mean tumor volume

of 300 mm³, the animals were orally treated daily with different doses of **21** (5, 10 and 20 mg/kg QD).

The results are shown in Figure 10.

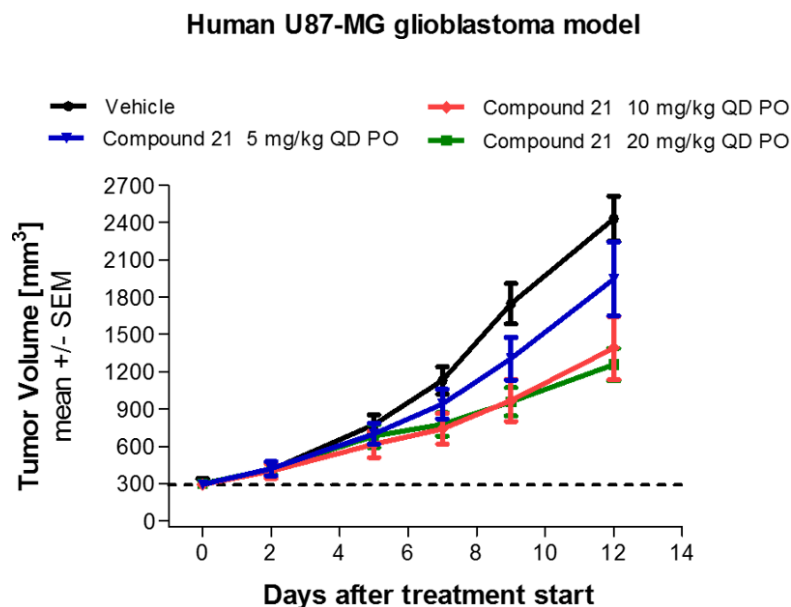


Figure 10: *in vivo* tumor growth inhibition of **21 in human U87-MG glioblastoma model. Tumor volumes for the 12-day treatment period (volumes for the individual animals at the end of the study are shown in the Supporting Information Figure S2).**

Dose dependent anti-tumor activity could be shown with compound **21**. Best efficacy was achieved at doses of 10 and 20 mg/kg daily (T/C value of 45%), while the lowest dose of 5 mg/kg resulted in a T/C value of 78%. Applying the highest daily dose but using an alternative scheduling (10 mg/kg BID) did not enhance the anti-tumor activity. All regimens were well tolerated, and no body weight loss was observed during the treatment period of 12 days (data not shown).

Conclusion

The anti-angiogenic properties of the natural product fumagillin were discovered already in 1990.²⁹ However, it took seven additional years until the molecular target of this compound class could be identified.³⁰ Since then many covalent and reversible ligands were investigated to understand the target biology and develop new drugs for indications with high medical need like cancer or obesity. For the latter condition at least one NCE (ZGN-1061) is in active clinical development. Compelling data render

1
2
3
4
5
6 MetAP-2 to be also a promising drug target for oncology. All clinical investigations in oncology so far
7
8 were only considering derivatives of fumagillin were discontinued due to unknown reasons. Using a
9
10 structure-based approach the successful optimization of the screening hit **11a** resulted in the advanced
11
12 lead **21** which was well tolerated and showed anti-tumor efficacy in a mouse glioblastoma model.
13
14 Furthermore, the derivative **21** set the basis for further optimizations to establish the clinical compound
15
16 M8891.
17

18 **Experimental Section**

21 **Chemistry** General Information. All reactions were carried out under nitrogen atmosphere or in sealed
22
23 vials unless noted otherwise. Dry solvents and reagents were of commercial quality and were used as
24
25 purchased. Reactions were magnetically stirred and monitored by thin-layer chromatography (TLC) using
26
27 Merck silica gel 60 F254 by fluorescence quenching under UV light or by high-pressure liquid
28
29 chromatography with subsequent mass detection (LCMS) detection, except if indicated otherwise.
30
31 LCMS-Analysis: Method A: A-0.1 % TFA in H₂O, B-0.1 % TFA in ACN: flow: 2.0 mL/min, column: XBridge C8
32
33 (50 x 4.6 mm, 3.5 μm), +ve mode. Method B: A- 0.1% HCOOH, B- Methanol: flow: 1.0 ml/min, column:
34
35 Eclipse plus C18 (50 x 4.6 mm); Method C: A- 0.1% HCOOH, B- Acetonitrile: flow: 1.0ml/min, column:
36
37 Atlantis dC18 (50 x 4.6 mm.) + ve mode. HPLC-analysis: A-0.1 % TFA in H₂O, B-0.1 % TFA in ACN: flow: 2.0
38
39 mL/min, column: XBridge C8 (50 x 4.6 mm, 3.5 μm). Chiral HPLC analysis: Method A: Mobile phase: 0.1%
40
41 DEA in hexane/IPA = 60:40, column: Chiralpak AD-H (250 x 4.6) mm, 5 μm, flow: 1.0mL\min; Method B:
42
43 Mobile phase: n-heptane/IPA = 60:40, column: Chiralpak AD-H (250 x 4.6) mm, 5 μm, flow: 1.0 mL/min;
44
45 Method C: Mobile phase: 0.1% TFA in hexane/IPA = 80:20, column: Chiralcel OJ-H (250 x 4.6) mm, 5 μm,
46
47 flow: 1.0mL/min; Method D: Mobile phase: heptane/IPA = 50:50, column: Chiralpak AD-H (250 x 4.6)
48
49 mm, 5 μm, flow rate: 0.8mL\min; Method E: Mobile phase: 0.1% DEA in hexane/IPA = 70:30, column:
50
51 Chiralpak AD-H (250 x 4.6) mm, 5 μm, flow: 1.0mL\min; Method F: Mobile phase: 0.1% DEA in
52
53 hexane/IPA = 70:30, column: Chiralpak OD-H (250 x 4.6) mm, 5 μm, flow: 1.0mL\min; Method G: Mobile
54
55 phase: hexane/IPA = 70:30, column: Chiralpak AD-H (250 x 4.6) mm, 5 μm, flow rate: 1.0mL\min.
56
57
58
59
60

Retention times (Rt) are given in minutes. In addition, TLC plates were stained using phosphomolybdic acid or potassium permanganate stain. Chromatographic purification of products (flash chromatography) was performed on Isco Combiflash systems using Rediseq columns and ethyl acetate/heptanes gradients. Concentration under reduced pressure was performed by rotary evaporation at 40 °C at the appropriate pressure unless otherwise stated. The purity of the compounds reported in the manuscript was established through HPLC-MS methodology. HPLC analyses were run according to the LCMS method. ¹H NMR (in DMSO-d₆) and mass spectra are in agreement with the structures and were recorded on a Bruker NMR 400 MHz spectrometer if not stated differently (Tetramethylsilane as an internal standard) and Vacuum Generators VG 70-70 or 70-250 at 70 eV, respectively. Elemental analyses (obtained with a Perkin-Elmer 240 BCHN analyzer) for the final products were within 0.4% of calculated values if not stated otherwise. All compounds reported in the manuscript have a purity ≥95% unless noted otherwise.

(S)-3-Hydroxy-2-oxo-1-phenyl-pyrrolidine-3-carboxylic acid (2-thiophen-2-yl-ethyl)-amide (S-11a)

Synthesis of 2-oxo-1-phenyl-N-[2-(thiophen-2-yl)ethyl]pyrrolidine-3-carboxamide

1-Phenyl-2-oxo-3-pyrrolidine carboxylic acid (200 mg, 0.95 mmol), 2-(thiophen-2-yl)-ethan-1-amine hydrochloride (155 mg, 0.95 mmol), EDCI (549 mg, 2.84 mmol), HOBt (192 mg, 1.42 mmol) and TEA (132 μL, 0.95 mmol) were dissolved in DMF (5 mL) and heated in the microwave to 160°C for 5 min. After the addition of water, the precipitate was filtered and dried, giving the product in 80 % (239 mg) yield as colorless solid.

Synthesis of 3-hydroxy-2-oxo-1-phenyl-N-[2-(thiophen-2-yl)ethyl]pyrrolidine-3-carboxamide

2-Oxo-1-phenyl-N-[2-(thiophen-2-yl)ethyl]pyrrolidine-3-carboxamide (100 mg, 0.32 mmol), tert-butyl hydro peroxide (70 % in water, 62 mg, 0.48 mmol) and sodium ethylate (20 % in ethanol, 182 μL, 0.48 mmol) were mixed with tert-butanol (10 ml) and heated to 90°C for 4 h. After concentration in vacuum the residue was distributed between ethyl acetate and water, the organic phase dried over Na₂SO₄, filtered and after removal of the solvent purified by chromatography, giving the product in 54 % (57 mg) yield. 3-Hydroxy-2-oxo-1-phenyl-N-[2-(thiophen-2-yl)ethyl]pyrrolidine-3-carboxamide (40 mg) was

1
2
3
4
5
6 separated into the enantiomers via chiral HPLC (ChiralCel OH; n-heptane/methanol = 7:3, giving *S*-**11a** in
7
8 51 % (20 mg) yield. Rt 7.19 min. ¹H NMR (500 MHz, DMSO-d₆) δ 8.08 (t, *J* = 5.9, 1H), 7.71 (s, 1H), 7.69 (d,
9
10 *J* = 8.8, 1H), 7.48 – 7.37 (m, 2H), 7.33 (dt, *J* = 10.3, 5.1, 1H), 7.23 – 7.13 (m, 1H), 6.96 (dd, *J* = 5.0, 3.5, 1H),
11
12 6.90 (t, *J* = 7.1, 1H), 6.61 (d, *J* = 17.5, 1H), 3.91 – 3.80 (m, 2H), 3.48 – 3.38 (m, 1H), 3.33 – 3.22 (m, 3H),
13
14 2.98 (t, *J* = 7.3, 2H), 2.58 – 2.52 (m, 1H), 2.10 (m, 1H); HRMS calcd for C₁₇H₁₉N₂O₃S (M+H⁺) 331.1111
15
16 found 331.1118. *R*-**11a** was also obtained in 51 % (20 mg) yield. Rt 15.21 min. HRMS calcd for
17
18 C₁₇H₁₉N₂O₃S (M+H⁺) 331.1111 found 331.1119.

19
20
21 Compounds **11b-11r** were prepared as described below:

22
23 To a solution of (*R*)-3-hydroxy-2-oxo-1-phenyl-pyrrolidine-3-carboxylic acid **16** (800 mg, 3.62mmol) and
24
25 the respective amine (4.34 mmol) in dry DMF was added EDCI (2.07 g, 10.86 mmol) and HOBt (731 mg,
26
27 5.43 mmol). The reaction mass was heated for 20 min at 160°C under microwave. After completion of
28
29 the reaction, DMF was removed under vacuum. The residue was diluted with water and extracted with
30
31 ethyl acetate. The organic layer was dried over Na₂SO₄ and concentrated under reduced pressure. The
32
33 crude was purified by flash column chromatography to afford the title compounds.

34
35
36 *(S)*-3-Hydroxy-2-oxo-1-phenyl-pyrrolidine-3-carboxylic acid [2-(5-methyl-thiophen-2-yl)-ethyl]-amide (**11b**)

37
38 The title compound was obtained in 15 % (12 mg) yield as light brown solid.

39
40
41 ¹H NMR (400 MHz, DMSO) δ 8.07 (t, *J* = 5.9, 1H), 7.73 – 7.65 (m, 2H), 7.40 (dd, *J* = 10.8, 5.3, 2H), 7.17 (t, *J*
42
43 = 7.4, 1H), 6.64 (d, *J* = 3.3, 1H), 6.63 (s, 1H), 6.59 (dd, *J* = 3.3, 1.1, 1H), 3.91 – 3.75 (m, 2H), 3.30 – 3.33 (m,
44
45 1H), 3.15 (m, 1H), 2.85 (t, *J* = 7.4, 2H), 2.53 (m, 1H), 2.34 (s, 3H), 2.07 (dt, *J* = 12.9, 8.0, 1H). LCMS:

46
47 (Method A) 345.3 (M+H), Rt 3.85 min, 99.16 (max), 98.99 (254nm); HPLC: Rt 3.92 min, 98.77 (max), 98.67
48
49 (254nm); HRMS calcd for C₁₈H₂₁N₂O₃S (M+H⁺) 345.1267 found 345.1274.

50
51
52 *(S)*-3-Hydroxy-2-oxo-1-phenyl-pyrrolidine-3-carboxylic acid (thiophen-2-ylmethyl)-amide (**11c**)

53
54 The title compound was obtained in 47 % (44 mg) yield as off white solid.

55
56
57 ¹H NMR (400 MHz, DMSO) δ 8.58 (t, *J* = 6.2, 1H), 7.70 (d, *J* = 1.1, 1H), 7.68 (d, *J* = 1.0, 1H), 7.45 – 7.33 (m,
58
59 3H), 7.22 – 7.14 (m, 1H), 6.99 – 6.87 (m, 2H), 6.66 (s, 1H), 4.44 (d, *J* = 6.4, 2H), 3.91 – 3.78 (m, 2H), 2.59 –
60

2.52 (m, 1H), 2.09 (dt, $J = 12.9, 8.5$, 1H). LCMS: (Method A) 317 (M+H), Rt 3.34 min, 96.06 (max), 98.75 (254nm); HPLC: Rt 3.28 min, 98.41 (max), 99.10 (254nm); Chiral HPLC: (Method B) Rt 6.57 min, area % 99.05 (210nm); HRMS calcd. for $C_{16}H_{16}N_2O_3S$ (M+H⁺) 317.0954 found 317.0966.

(S)-3-Hydroxy-2-oxo-1-phenyl-pyrrolidine-3-carboxylic acid (3-methyl-thiophen-2-ylmethyl)-amide (11d)

The title compound was obtained in 46 % (45 mg) yield as off white solid.

¹H NMR (400 MHz, DMSO) δ 8.45 (t, $J = 6.1$, 1H), 7.74 – 7.66 (m, 2H), 7.46 – 7.37 (m, 2H), 7.25 (d, $J = 5.1$, 1H), 7.22 – 7.14 (m, 1H), 6.79 (d, $J = 5.1$, 1H), 6.64 (s, 1H), 4.39 (dd, $J = 15.2, 6.4$, 1H), 4.33 (dd, $J = 15.4, 6.4$, 1H), 3.84 (ddd, $J = 14.2, 9.2, 3.7$, 2H), 2.60 – 2.52 (m, 1H), 2.16 (s, 3H), 2.09 (dt, $J = 12.9, 8.5$, 1H).

LCMS: (Method A) 331 (M+H), Rt 3.52 min, 96.54 (max), 95.65 (254nm); HPLC: (Method A) Rt 3.65 min, 96.02 (max), 94.41 (254nm); HRMS calcd for $C_{17}H_{19}N_2O_3S$ (M+H⁺) 331.1111 found 331.1117.

(S)-3-Hydroxy-2-oxo-1-phenyl-pyrrolidine-3-carboxylic acid (4-methyl-thiophen-2-ylmethyl)-amide (11e)

The title compound was obtained in 52 % (43 mg) yield as off white solid.

¹H NMR (400 MHz, DMSO) δ 8.52 (t, $J = 6.2$, 1H), 7.70 (dd, $J = 5.4, 3.4$, 2H), 7.44 – 7.37 (m, 2H), 7.22 – 7.14 (m, 1H), 6.94 – 6.90 (m, 1H), 6.76 (s, 1H), 6.66 (s, 1H), 4.45 – 4.30 (m, 2H), 3.93 – 3.78 (m, 2H), 2.56 – 2.51 (m, 1H), 2.13 (s, 3H), 2.12 – 2.05 (m, 1H). LCMS: (Method A) 331 (M+H), Rt 3.74 min, 92.09 (max), 92.33 (254nm); HPLC: Rt 3.66 min, 96.29(max), 96.27(254nm); HRMS calcd for $C_{17}H_{19}N_2O_3S$ (M+H⁺) 331.1111 found 331.1121.

(S)-3-Hydroxy-2-oxo-1-phenyl-pyrrolidine-3-carboxylic acid (5-methyl-thiophen-2-ylmethyl)-amide (11f)

The title compound was obtained in 44 % (37 mg) yield as off white solid.

¹H NMR (400 MHz, DMSO) δ 8.48 (t, $J = 6.2$, 1H), 7.69 (dd, $J = 8.7, 1.1$, 2H), 7.44 – 7.36 (m, 2H), 7.23 – 7.09 (m, 1H), 6.71 (d, $J = 3.3$, 1H), 6.65 (s, 1H), 6.63 – 6.54 (m, 1H), 4.44 – 4.28 (m, 2H), 3.92 – 3.76 (m, 2H), 2.57 – 2.51 (m, 1H), 2.36 (d, $J = 0.8$, 3H), 2.15 – 2.04 (m, 1H). LCMS: (Method C) 331 (M+H), Rt 2.52 min, 91.54 (max); HPLC: Rt 3.65 min, 92.26 (max), 90.62 (254nm); HRMS calcd for $C_{17}H_{19}N_2O_3S$ (M+H⁺) 331.1111 found 331.1118.

(S)-3-Hydroxy-2-oxo-1-phenyl-pyrrolidine-3-carboxylic acid (2-furan-2-yl-ethyl)-amide (11g)

1
2
3
4
5
6 The title compound was obtained in 51 % (50 mg) yield as white solid

7
8 ^1H NMR (400 MHz, DMSO) δ 8.06 (t, J = 5.9, 1H), 7.70 (t, J = 1.5, 1H), 7.68 (t, J = 1.6, 1H), 7.52 (dd, J = 1.8,
9 0.7, 1H), 7.44 – 7.37 (m, 2H), 7.22 – 7.14 (m, 1H), 6.62 (s, 1H), 6.35 (dd, J = 3.1, 1.9, 1H), 6.16 (dd, J = 3.1,
10 0.7, 1H), 3.92 – 3.76 (m, 2H), 3.40 (td, J = 13.7, 7.4, 1H), 2.79 (t, J = 7.3, 2H), 2.53 (dd, J = 6.7, 3.6, 1H),
11 2.15 – 2.00 (m, 1H). HRMS calcd for $\text{C}_{17}\text{H}_{19}\text{N}_2\text{O}_4$ ($\text{M}+\text{H}^+$) 315.1339 found 315.1348.

12
13
14
15
16 *(S)*-3-Hydroxy-2-oxo-1-phenyl-pyrrolidine-3-carboxylic acid (2-cyclopentyl-ethyl)-amide (**11h**)

17
18
19 The title compound was obtained in 53 % (38 mg) yield as off white solid.

20
21 ^1H NMR (400 MHz, DMSO) δ 8.72 (t, J = 6.4, 1H), 7.69 (dd, J = 8.7, 1.0, 2H), 7.45 – 7.33 (m, 2H), 7.27 (dt, J
22 = 8.8, 2.1, 1H), 7.18 (dd, J = 13.0, 4.5, 2H), 7.10 (d, J = 9.0, 1H), 6.76 (s, 1H), 4.38 (dd, J = 15.7, 6.6, 1H),
23 4.24 (dd, J = 15.9, 6.0, 1H), 3.89 – 3.82 (m, 2H), 2.62 – 2.54 (m, 1H), 2.12 (dt, J = 12.9, 7.6, 1H); LCMS:
24 (Method A) 317.0 ($\text{M}+\text{H}$), Rt 4.03 min, 96.61 (max), 98.74 (254nm); HPLC: Rt 4.1 min, 97.63(max), 98.56
25 (254nm); Chiral HPLC: (Method G) Rt 5.52 min Area % 100 (210nm); HRMS calcd for $\text{C}_{18}\text{H}_{25}\text{N}_2\text{O}_3$ ($\text{M}+\text{H}^+$)
26 317.186 found 317.1868.

27
28
29
30
31
32
33 *(S)*-3-Hydroxy-2-oxo-1-phenyl-pyrrolidine-3-carboxylic acid benzylamide (**11i**)

34
35
36 The title compound was obtained in 15 % (12 mg) yield as light brown solid.

37
38 ^1H NMR (400 MHz, DMSO) δ 8.51 (t, J = 6.0, 1H), 7.69 (dd, J = 8.6, 0.9, 2H), 7.45 – 7.34 (m, 2H), 7.32 –
39 7.24 (m, 4H), 7.20 (dt, J = 14.8, 4.6, 2H), 6.68 (s, 1H), 4.33 (dd, J = 15.1, 6.5, 1H), 4.27 (dd, J = 15.1, 6.2,
40 1H), 3.92 – 3.74 (m, 2H), 2.63 – 2.52 (m, 2H), 2.11 (dt, J = 12.9, 7.9, 1H); LCMS: (Method A) 311.3 ($\text{M}+\text{H}$),
41 Rt 3.29 min, 99.74 (max), 99.55 (254nm); HPLC: (Method A) Rt 3.93 min, 98.92 (max), 99.61 (254nm);
42 Chiral HPLC: (Method E) Rt 8.81 min Area % 100 (210nm); HRMS calcd for $\text{C}_{18}\text{H}_{19}\text{N}_2\text{O}_3$ ($\text{M}+\text{H}^+$) 311.139
43 found 311.1399.

44
45
46
47
48
49
50
51 *(S)*-3-Hydroxy-2-oxo-1-phenyl-pyrrolidine-3-carboxylic acid 2-chloro-benzylamide (**11j**)

52
53
54 The title compound was obtained in 37 % (26 mg) yield as brown gum.

55
56 ^1H NMR (400 MHz, DMSO) δ 8.59 (t, J = 6.3, 1H), 7.70 (dt, J = 9.0, 1.7, 2H), 7.44 – 7.24 (m, 6H), 7.21 – 7.14
57 (m, 1H), 6.79 (s, 1H), 4.41 (dd, J = 16.2, 6.5, 1H), 4.31 (dd, J = 16.1, 6.1, 1H), 3.86 (dd, J = 8.5, 5.6, 2H),
58
59
60

2.65 – 2.57 (m, 1H), 2.14 (dt, $J = 12.9, 7.7$, 1H); HRMS calcd for $C_{18}H_{18}ClN_2O_3$ ($M+H^+$) 345.1 found 345.1004.

(S)-3-Hydroxy-2-oxo-1-phenyl-pyrrolidine-3-carboxylic acid 3-chloro-benzylamide (**11k**)

The title compound was obtained in 34 % (27 mg) yield as brown solid.

1H NMR (400 MHz, DMSO) δ 8.65 (t, $J = 6.2$, 1H), 7.69 (dd, $J = 8.7, 1.1$, 2H), 7.43 – 7.37 (m, 2H), 7.33 (t, $J = 7.6, 2H$), 7.27 (dd, $J = 6.6, 2.1$, 1H), 7.22 (d, $J = 7.5$, 1H), 7.18 (dd, $J = 10.5, 4.2$, 1H), 6.73 (s, 1H), 4.35 (dd, $J = 15.2, 6.6$, 1H), 4.25 (dd, $J = 15.4, 6.1$, 1H), 3.90 – 3.80 (m, 2H), 2.61 – 2.54 (m, 1H), 2.11 (dt, $J = 13.0, 7.8$, 1H); LCMS: (Method A) 345 ($M+H$), Rt 3.86 min, 93.21 (max), 98.65 (254nm); HPLC: Rt 3.93 min, 90.93 (max), 98.60 (254nm); Chiral HPLC: (Method D) Rt 8.26 min, area % 93.34 (210nm); HRMS calcd for $C_{18}H_{18}ClN_2O_3$ ($M+H^+$) 345.1 found 345.1004.

(S)-3-Hydroxy-2-oxo-1-phenyl-pyrrolidine-3-carboxylic acid 4-chloro-benzylamide (**11l**)

The title compound was obtained in 37 % (27 mg) yield as off white solid.

1H NMR (400 MHz, DMSO) δ 8.60 (t, $J = 6.3$, 1H), 7.69 (dt, $J = 8.9, 1.7$, 2H), 7.43 – 7.33 (m, 4H), 7.31 – 7.25 (m, 2H), 7.21 – 7.13 (m, 1H), 6.70 (s, 1H), 4.31 (dd, $J = 15.2, 6.5$, 1H), 4.24 (dd, $J = 15.2, 6.2$, 1H), 3.91 – 3.76 (m, 2H), 2.56 (ddd, $J = 12.8, 7.1, 4.4$, 1H), 2.17 – 2.04 (m, 1H); HRMS calcd for $C_{18}H_{18}ClN_2O_3$ ($M+H^+$) 345.1 found 345.1004.

(S)-3-Hydroxy-2-oxo-1-phenyl-pyrrolidine-3-carboxylic acid 2-fluoro-benzylamide (**11m**)

The title compound was obtained in 25 % (17 mg) yield as brown gum.

1H NMR (400 MHz, DMSO) δ 8.53 (t, $J = 6.3$, 1H), 7.73 – 7.66 (m, 2H), 7.43 – 7.37 (m, 2H), 7.34 (t, $J = 7.8$, 1H), 7.31 – 7.25 (m, 1H), 7.20 – 7.11 (m, 3H), 6.73 (s, 1H), 4.38 (dd, $J = 15.6, 6.4$, 1H), 4.31 (dd, $J = 15.5, 5.9$, 1H), 3.91 – 3.80 (m, 2H), 2.58 (ddd, $J = 12.9, 7.0, 4.5$, 1H), 2.12 (dt, $J = 13.0, 7.7$, 1H); HRMS calcd for $C_{18}H_{18}FN_2O_3$ ($M+H^+$) 329.1296 found 329.1303.

(S)-3-Hydroxy-2-oxo-1-phenyl-pyrrolidine-3-carboxylic acid 3-fluoro-benzylamide (**11n**)

The title compound was obtained in 44 % (34 mg) yield as brown solid.

¹H NMR (400 MHz, DMSO) δ 8.64 (t, *J* = 6.4, 1H), 7.69 (dd, *J* = 8.7, 1.1, 2H), 7.43 – 7.37 (m, 2H), 7.33 (td, *J* = 7.9, 6.1, 1H), 7.21 – 7.14 (m, 1H), 7.10 (d, *J* = 7.4, 2H), 7.08 – 6.99 (m, 2H), 6.73 (s, 1H), 4.37 (dd, *J* = 15.5, 6.6, 1H), 4.26 (dd, *J* = 15.4, 6.1, 1H), 3.92 – 3.75 (m, 2H), 2.63 – 2.54 (m, 1H), 2.12 (dt, *J* = 12.9, 7.7, 1H). LCMS: (Method A) 329 (M+H), Rt 3.50 min, 94.01(max), 96.23(254nm); HPLC: Rt 3.66 min, 91.55 (max), 94.61 (254nm); Chiral HPLC: (Method D) Rt 7.14 min, area % 93.67 (210nm); HRMS calcd for C₁₈H₁₈FN₂O₃ (M+H⁺) 329.1296 found 329.1305.

(S)-3-Hydroxy-2-oxo-1-phenyl-pyrrolidine-3-carboxylic acid 3-methyl-benzylamide (**11o**)

The title compound was obtained in 10 % (7 mg) yield as light brown solid.

¹H NMR (400 MHz, DMSO) δ 8.46 (t, *J* = 6.2, 1H), 7.70 (d, *J* = 7.8, 2H), 7.46 – 7.35 (m, 2H), 7.17 (t, *J* = 7.3, 2H), 7.07 (d, *J* = 4.4, 2H), 7.02 (d, *J* = 7.8, 1H), 6.68 (s, 1H), 4.29 (dd, *J* = 15.0, 6.5, 1H), 4.23 (dd, *J* = 15.1, 6.2, 1H), 3.96 – 3.74 (m, 2H), 2.64 – 2.52 (m, 1H), 2.26 (s, 3H), 2.11 (dt, *J* = 12.8, 7.8, 1H). LCMS: (Method A) 325.3 (M+H), Rt 3.74 min, 99.67 (max), 99.56 (254nm); HPLC: Rt 3.78 min, 98.77 (max), 99.48 (254nm); HRMS calcd for C₁₉H₂₁N₂O₃ (M+H⁺) 325.1547 found 325.1557.

(S)-3-Hydroxy-2-oxo-1-phenyl-pyrrolidine-3-carboxylic acid 3,5-dichloro-benzylamide (**11p**)

The title compound was obtained in 40 % (35 mg) yield as brown solid.

¹H NMR (400 MHz, DMSO) δ 8.74 (t, *J* = 6.4, 1H), 7.70 (dd, *J* = 8.7, 1.0, 2H), 7.45 (t, *J* = 1.9, 1H), 7.44 – 7.36 (m, 2H), 7.32 (d, *J* = 1.9, 2H), 7.18 (t, *J* = 7.4, 1H), 6.77 (s, 1H), 4.37 (dd, *J* = 15.6, 6.7, 1H), 4.23 (dd, *J* = 15.7, 6.0, 1H), 3.90 – 3.78 (m, 2H), 2.63 – 2.53 (m, 1H), 2.12 (dt, *J* = 13.0, 7.7, 1H); LCMS: (Method A) 379 (M+H), Rt 4.43 min, 92.92 (max), 96.66 (254nm); HPLC: Rt 4.43 min, 96.87 (max), 98.91 (254nm); HRMS calcd for C₁₈H₁₇Cl₂N₂O₃ (M+H⁺) 379.0611 found 379.0621.

(S)-3-Hydroxy-2-oxo-1-phenyl-pyrrolidine-3-carboxylic acid 3,5-difluoro-benzylamide (**11q**)

The title compound was obtained in 56 % (54 mg) yield as off white solid.

¹H NMR (400 MHz, DMSO) δ 8.72 (t, *J* = 6.4, 1H), 7.73 – 7.67 (m, 2H), 7.43 – 7.37 (m, 2H), 7.18 (dd, *J* = 10.5, 4.2, 1H), 7.06 (tt, *J* = 9.4, 2.4, 1H), 7.00 – 6.95 (m, 2H), 6.77 (s, 1H), 4.39 (dd, *J* = 15.9, 6.8, 1H), 4.24 (dd, *J* = 15.8, 6.0, 1H), 3.86 (dd, *J* = 8.0, 5.7, 2H), 2.63 – 2.55 (m, 1H), 2.18 – 2.07 (m, 1H). LCMS: (Method

1
2
3
4
5
6 A) 347.2 (M+H), Rt 3.86 min, 90.39(max), 94.47(254nm); HPLC: Rt 3.82 min, 92.48 (max), 92.88 (254nm);

7
8 Chiral HPLC: (Method B) Rt 5.14 min Area % 99.84(210nm); HRMS calcd for C₁₈H₁₇F₂N₂O₃ (M+H⁺)

9
10 347.1202 found 347.1206.

11
12 *(S)*-3-Hydroxy-2-oxo-1-phenyl-pyrrolidine-3-carboxylic acid 3-chloro-5-fluoro-benzylamide (**11r**)

13
14 The title compound was obtained in 55 % (43 mg) yield as off white solid.

15
16 ¹H NMR (400 MHz, DMSO-d₆) δ 8.72 (t, *J* = 6.36 Hz, 1H), 7.69 (d, *J* = 7.84 Hz, 2H), 7.40 (t, *J* = 8.36 Hz, 2H),
17
18 7.28-7.25 (m, 1H), 7.20-7.16 (m, 2H), 7.11-7.09 (m, 1H), 6.76 (s, 1H), 4.41-4.35 (m, 1H), 4.27-4.22 (m, 1H),
19
20 3.86 (t, *J* = 7.44 Hz, 2H), 2.62-2.55 (m, 1H), 2.16-2.09 (m, 1H). LCMS: (Method A) 363 (M+H), Rt 4.02 min,
21
22 97.87(max); 99.35(254nm). HPLC: Rt 4.12 min, 97.88 (max); 99.35 (254nm). Chiral HPLC: (Method C) Rt
23
24 (min): 12.10 Area % 100. HRMS calcd for C₁₈H₁₇ClFN₂O₃ (M+H⁺) 363.0906 found 363.0907.

25
26
27 Compounds **11ra** – **11rj** were prepared according to the following general protocol:

28
29 *(R)*-3-Hydroxy-2-oxo-pyrrolidine-3-carboxylic acid 3-chloro-5-fluoro-benzylamide (*R*-**18**; 70 mg; 0.24
30
31 mmol) and the respective aryl halogenide (0.29 mmol) were dissolved in dry 1,4-Dioxan (4 ml) and
32
33 purged with nitrogen for 10min. Then K₂CO₃ (101 mg; 0.73 mmol), CuI (186 mg; 0.98 mmol) and N,N'-
34
35 Dimethylethylenediamin (0.13 ml; 1.22 mmol) were added to the reaction mixture and heated to 100°C
36
37 for 2 days. Then the reaction was filtered and washed with DCM and MeOH. The filtrate was extracted
38
39 with DCM/water. The organic layer was dried over MgSO₄, filtered and evaporated in vacuo. The
40
41 product was purified on prep. HPLC.

42
43 *(S)*-3-Hydroxy-2-oxo-1-*o*-tolyl-pyrrolidine-3-carboxylic acid 3-chloro-5-fluoro-benzylamide (**11ra**)

44
45 The title compound was obtained in 23 % (43 mg) yield as white solid.

46
47 ¹H NMR (400 MHz, DMSO-d₆) δ 8.69 (t, *J* = 6.4, 1H), 7.32 – 7.17 (m, 6H), 7.11 (d, *J* = 9.7, 1H), 6.70 (s, 1H),
48
49 4.41 (dd, *J* = 15.9, 6.7, 1H), 4.24 (dd, *J* = 15.8, 6.0, 1H), 3.68 (dd, *J* = 8.3, 5.3, 2H), 2.65 – 2.57 (m, 1H), 2.19
50
51 (dt, *J* = 13.0, 7.6, 1H), 2.11 (s, 3H); LCMS: (Method A) 377.0 (M+H), Rt 4.16 min, 96.51(max), 96.73
52
53 (220nm). HPLC: Rt 4.97 min, 99.09 (max), 98.88 (220nm); Chiral HPLC (after prep): (Method B) Rt 5.15
54
55 min; area % 99.16; HRMS calcd for C₁₉H₁₉ClFN₂O₃ (M+H⁺) 377.1063 found 377.1068.
56
57
58
59
60

1
2
3
4
5
6 (S)-3-Hydroxy-2-oxo-1-m-tolyl-pyrrolidine-3-carboxylic acid 3-chloro-5-fluoro-benzylamide (**11rb**)
7

8 The title compound was obtained in 9 % (24 mg) yield as colorless gum.

9
10 ¹H NMR (400 MHz, DMSO-d₆) δ 8.72 (t, *J* = 6.3, 1H), 7.50 (d, *J* = 6.5, 2H), 7.31 – 7.24 (m, 2H), 7.20 (s, 1H),
11
12 7.10 (d, *J* = 9.7, 1H), 7.00 (d, *J* = 7.3, 1H), 6.74 (s, 1H), 4.38 (dd, *J* = 15.8, 6.7, 1H), 4.23 (dd, *J* = 15.7, 6.0,
13
14 1H), 3.83 (dd, *J* = 8.0, 5.6, 2H), 2.63 – 2.53 (m, 1H), 2.11 (dt, *J* = 13.0, 7.6, 1H); LCMS: (Method A) 377.0
15
16 (M+H), Rt 4.16 min, 96.51 (max), 96.73 (220nm). HPLC: Rt 4.44 min, 96.29 (max), 97.81 (254nm); Chiral
17
18 HPLC (after prep): (Method B) Rt 5.18 min, area % 99.85; HRMS calcd for C₁₉H₁₉ClFN₂O₃ (M+H⁺)
19
20 377.1063 found 377.1069.
21
22

23 (S)-3-Hydroxy-2-oxo-1-p-tolyl-pyrrolidine-3-carboxylic acid 3-chloro-5-fluoro-benzylamide (**11rc**)
24

25 The title compound was obtained in 15 % (32 mg) yield as white solid.

26
27 ¹H NMR (400 MHz, DMSO-d₆) δ 8.72 (t, *J* = 6.4, 1H), 7.60 – 7.55 (m, 2H), 7.27 (dt, *J* = 8.8, 2.2, 1H), 7.20
28
29 (dd, *J* = 4.9, 3.3, 3H), 7.10 (d, *J* = 9.7, 1H), 6.73 (s, 1H), 4.37 (dd, *J* = 15.8, 6.7, 1H), 4.23 (dd, *J* = 15.8, 6.0,
30
31 1H), 3.82 (dd, *J* = 7.5, 6.1, 2H), 2.63 – 2.54 (m, 1H), 2.28 (s, 3H), 2.10 (dt, *J* = 13.0, 7.6, 1H); LCMS:
32
33 (Method A) 377 (M+H), Rt 4.40 min, 97.39(max), 98.43(254nm); HPLC: (Method A) Rt 4.42 min, 98.42
34
35 (max), 98.40 (254nm); HRMS calcd for C₁₉H₁₉ClFN₂O₃ (M+H⁺) 377.1063 found 377.1064.
36
37

38 (S)-1-(2-Cyano-phenyl)-3-hydroxy-2-oxo-pyrrolidine-3-carboxylic acid 3-chloro-5-fluoro-benzylamide
39
40 (**11rd**)
41

42 The title compound was obtained in 9 % (18 mg) yield as off white solid.

43
44 ¹H NMR (400 MHz, DMSO-d₆) δ 8.74 (t, *J* = 6.5, 1H), 7.92 (dd, *J* = 8.0, 1.5, 1H), 7.84 – 7.74 (m, 1H), 7.51
45
46 (ddd, *J* = 6.3, 3.7, 1.1, 2H), 7.27 (dd, *J* = 8.8, 2.2, 1H), 7.21 (s, 1H), 7.11 (d, *J* = 8.8, 1H), 6.87 (s, 1H), 4.39
47
48 (dd, *J* = 15.7, 7.0, 1H), 4.26 (dd, *J* = 15.8, 6.2, 1H), 3.97 – 3.76 (m, 3H), 2.69 – 2.56 (m, 2H), 2.28 – 2.14 (m,
49
50 1H). LCMS: (Method A) 388.0 (M+H), Rt 3.83 min, 96.26 (max), 97.18 (254nm); HPLC: (Method A) Rt 3.87
51
52 min, 97.15 (max), 97.21 (254nm); Chiral HPLC (after prep): (Method B) Rt (min): 5.85 Area % 97.80;
53
54
55 HRMS calcd for C₁₉H₁₆ClFN₃O₃ (M+H⁺) 388.0859 found 388.0861.
56
57
58
59
60

1
2
3
4
5
6 *(S)*-1-(3-Cyano-phenyl)-3-hydroxy-2-oxo-pyrrolidine-3-carboxylic acid 3-chloro-5-fluoro-benzylamide

7
8 **(11re)**

9
10 The title compound was obtained in 12 % (11 mg) yield as brown gum.

11
12 ¹H NMR (400 MHz, DMSO-d₆) δ 8.78 (t, *J* = 6.3, 1H), 8.16 (s, 1H), 8.08 (dt, *J* = 7.4, 2.0, 1H), 7.68 – 7.59 (m,
13 2H), 7.27 (dd, *J* = 8.8, 2.0, 1H), 7.19 (s, 1H), 7.09 (d, *J* = 9.5, 1H), 6.86 (s, 1H), 4.38 (dd, *J* = 15.6, 6.7, 1H),
14 4.24 (dd, *J* = 15.7, 6.0, 1H), 3.96 – 3.84 (m, 2H), 2.59 (ddd, *J* = 11.8, 7.1, 4.5, 1H), 2.14 (dt, *J* = 13.1, 7.9,
15 1H). LCMS: (Method A) 388.3 (M+H), Rt 5.43 min, 96.54(max), 93.54(254nm); HPLC: (Method A) Rt 4.16
16 min, 94.60 (max), 92.61 (254nm); Chiral HPLC (after prep): (Method B) Rt (min): 6.39, area % 99.39;
17
18 HRMS calcd for C₁₉H₁₆ClFN₃O₃ (M+H⁺) 388.0859 found 388.0863.

19
20
21
22
23 *(S)*-1-(4-Cyano-phenyl)-3-hydroxy-2-oxo-pyrrolidine-3-carboxylic acid 3-chloro-5-fluoro-benzylamide

24
25
26
27 **(11rf)**

28
29 The title compound was obtained in 4 % (9 mg) yield as green solid.

30
31
32 ¹H NMR (400 MHz, DMSO-d₆) δ 8.79 (s, 1H), 7.91 (q, *J* = 9.1, 4H), 7.27 (d, *J* = 8.7, 1H), 7.19 (s, 1H), 7.08 (s,
33 1H), 6.88 (s, 1H), 4.37 (dd, *J* = 15.6, 6.2, 2H), 4.23 (dd, *J* = 15.7, 5.8, 2H), 3.90 (dd, *J* = 11.5, 5.7, 2H), 2.63 –
34 2.57 (m, 2H), 2.15 (dt, *J* = 11.6, 7.4, 2H). LCMS: (Method B) 388.3 (M-H), Rt.3.53min, 90.47(max),
35 90.32(254nm); HPLC: (Method A) Rt 4.15min, 90.20 (max), 94.77 (254nm); chiral HPLC (after prep):
36
37 (Method A) Rt 13.77 min; area % 97.70; HRMS calcd for C₁₉H₁₆ClFN₃O₃ (M+H⁺) 388.0859 found
38
39 388.0859.

40
41
42
43
44
45 *1*-(3-Acetylamino-phenyl)-3-hydroxy-2-oxo-pyrrolidine-3-carboxylic acid 3-chloro-5-fluoro-benzylamide

46
47 **(11rg)**

48
49 The title compound was obtained in 12 % (26 mg) yield as white solid.

50
51
52 ¹H NMR (400 MHz, DMSO-d₆) δ 10.02 (s, 1H), 8.73 (s, 1H), 7.93 (s, 1H), 7.48 – 7.43 (m, 1H), 7.34 – 7.24
53 (m, 3H), 7.20 (s, 1H), 7.09 (d, *J* = 9.7, 1H), 6.78 (s, 1H), 4.38 (dd, *J* = 15.7, 6.2, 1H), 4.24 (dd, *J* = 15.7, 5.3,
54 1H), 3.81 (dd, *J* = 8.3, 5.6, 2H), 2.62 – 2.53 (m, 1H), 2.12 (m, 1H), 2.03 (s, 3H). LCMS: (Method A) 420
55
56
57
58
59
60

(M+H), Rt 3.51min, 98.57 (max), 98.89 (254nm); HPLC: (Method A) Rt 3.46 min, 99.18 (max), 99.45 (254nm); HRMS calcd for C₂₀H₂₀ClFN₃O₄ (M+H⁺) 420.1121 found 420.1125.

(S)-1-(4-Acetylamino-phenyl)-3-hydroxy-2-oxo-pyrrolidine-3-carboxylic acid 3-chloro-5-fluoro-benzylamide (**11rh**)

The title compound was obtained in 7 % (4 mg) yield as pale brown solid.

¹H NMR (400 MHz, DMSO-d₆) δ 9.96 (s, 1H), 8.71 (t, *J* = 6.5, 1H), 7.66 – 7.55 (m, 4H), 7.27 (d, *J* = 8.5, 1H), 7.20 (s, 1H), 7.09 (d, *J* = 9.2, 1H), 6.73 (s, 1H), 4.38 (dd, *J* = 15.4, 6.6, 1H), 4.23 (dd, *J* = 15.7, 5.9, 1H), 3.81 (t, *J* = 6.8, 2H), 2.62 – 2.53 (m, 2H), 2.16 – 2.05 (m, 2H), 2.02 (s, 3H). LCMS: (Method A) 420.0 (M+H), Rt 3.34min, 97.16 (max), 97.53 (254nm); HPLC: (Method A) Rt 3.41 min, 99.24 (max), 99.56 (254nm); HRMS calcd. for C₂₀H₂₀ClFN₃O₄ (M+H⁺) 420.1121 found 420.1128.

(S)-1-(3-Carbamoyl-phenyl)-3-hydroxy-2-oxo-pyrrolidine-3-carboxylic acid 3-chloro-5-fluoro-benzylamide (**11ri**)

The title compound was obtained in 30 % (108 mg) yield as white solid.

¹H NMR (400 MHz, DMSO-d₆) δ 8.75 (t, *J* = 6.4, 1H), 8.07 – 8.00 (m, 2H), 7.99 – 7.93 (m, 1H), 7.67 (d, *J* = 7.9, 1H), 7.48 (t, *J* = 8.0, 1H), 7.42 (s, 1H), 7.27 (dt, *J* = 8.8, 2.2, 1H), 7.20 (s, 1H), 7.10 (d, *J* = 9.7, 1H), 6.80 (s, 1H), 4.38 (dd, *J* = 15.8, 6.7, 1H), 4.25 (dd, *J* = 15.7, 6.0, 1H), 3.94 – 3.86 (m, 2H), 2.64 – 2.56 (m, 1H), 2.14 (dt, *J* = 13.0, 7.6, 1H). LCMS: (Method A) 406(M+H), Rt 3.23min, 95.75 (max), 97.17 (254nm); HPLC: (Method A) Rt 3.37 min, 96.31 (max), 97.52 (254nm); Chiral HPLC (after prep): (Method B) Rt 5.78 min; area % 97.96; HRMS calcd for C₁₉H₁₈ClFN₃O₄ (M+H⁺) 406.0964 found 406.0965.

(S)-1-(4-Carbamoyl-phenyl)-3-hydroxy-2-oxo-pyrrolidine-3-carboxylic acid 3-chloro-5-fluoro-benzylamide (**11rj**)

The title compound was obtained in 2 % (4 mg) yield as off white solid.

¹H NMR (400 MHz, DMSO-d₆) δ 8.76 (t, *J* = 6.4, 1H), 7.95 (br. s, 1H), 7.91 (d, *J* = 8.8, 2H), 7.79 (d, *J* = 8.9, 2H), 7.33 (br. s, 1H), 7.27 (d, *J* = 8.7, 1H), 7.20 (s, 1H), 7.10 (d, *J* = 9.2, 1H), 6.82 (s, 1H), 4.38 (dd, *J* = 15.8, 6.9, 1H), 4.24 (dd, *J* = 15.8, 6.0, 1H), 3.89 (dd, *J* = 9.3, 5.1, 2H), 3.37 (m, 1H), 2.64 – 2.55 (m, 2H), 2.19 –

1
2
3
4
5
6 2.08 (m, 1H). LCMS: (Method A) 406 (M+H), Rt 3.24min, 91.44 (max), 94.05 (254nm); HPLC: (Method A)
7
8 Rt 3.20 min, 92.44 (max), 95.13 (254nm); HRMS calcd for C₁₉H₁₈ClFN₃O₄ (M+H⁺) 406.0964 found
9
10 406.0969.

11 12 **2-Oxo-1-phenyl-pyrrolidine-3-carboxylic acid (13)**

13
14 Meldrum's acid **12** (10 g, 58.76 mmol) and aniline (10.9 g, 117.53 mmol) were mixed at rt and stirred for
15
16 12 h. The reaction mixture was basified with 10 % NaOH solution and again acidified with conc. HCl. The
17
18 precipitate was filtered through vacuum and dried to afford the title compound in 96 % yield (11.5 g,
19
20 yellow liquid). ¹H NMR (400 MHz, DMSO-d₆) δ 13.28 (brs, 1H), 7.64-7.62 (m, 2H), 7.40-7.36 (m, 2H), 7.18-
21
22 7.13 (m, 1H), 3.90-3.81 (m, 2H), 3.61-3.56 (m, 1H), 2.36-2.27 (m, 2H) LCMS: (Method A) 206.3 (M+H⁺), Rt
23
24 2.43 min, 93.18% (Max).

25 26 27 **2-Oxo-1-phenyl-pyrrolidine-3-carboxylic acid ethyl ester (14)**

28
29 To a solution of 2-Oxo-1-phenyl-pyrrolidine-3-carboxylic acid **13** (11 g, 53.65 mmol) in dry ethanol (150
30
31 mL) was added thionyl chloride (25.5 g, 214.6 mmol) slowly at 0°C under nitrogen. The reaction mass
32
33 slowly warmed to rt and was refluxed for 4h under nitrogen. After the completion of the reaction, the
34
35 reaction mixture was concentrated under reduced pressure to remove the solvent. The crude mixture
36
37 was diluted with water, basified with 10% NaHCO₃ solution and was extracted with ethyl acetate. The
38
39 organic layer was separated and washed with water and brine, dried over Na₂SO₄ and concentrated
40
41 under reduced pressure to afford the title compound in 92% (11.5 g) yield. ¹H NMR (400 MHz, DMSO-d₆)
42
43 δ =7.64-7.62 (m, 2H), 7.40-7.36 (m, 2H), 7.18-7.14 (m, 1H), 4.18-4.12 (m, 2H), 3.90-3.83 (m, 2H), 3.73 (t, *J*
44
45 = 8.88 Hz, 1H), 2.39-2.31 (m, 2H), 1.21 (t, *J* = 7.12 Hz, 3H). LCMS: (Method A) 234 (M+H⁺), Rt 3.46 min,
46
47 98.34% (Max); 97.54 (254nm).

48 49 50 51 **(R)-3-hydroxy-2-oxo-1-phenyl-pyrrolidine-3-carboxylic acid ethyl ester (R-15)**

52
53 To 2-oxo-1-phenyl-pyrrolidine-3-carboxylic acid ethyl ester **14** (11.5 g, 49.35 mmol) in IPA (100 mL) was
54
55 added cerium chloride heptahydrate (4.84 g, 49.65 mmol), the reaction mixture was degassed with O₂ for
56
57 15 min and allowed to stir for 12 h under O₂ atmosphere. After completion of the reaction as confirmed
58
59
60

1
2
3
4
5
6 from TLC the solvent was removed and the crude was purified by flash column chromatography. 3-
7
8 Hydroxy-2-oxo-1-phenyl-pyrrolidine-3-carboxylic acid ethyl ester (12 g) was analyzed in chiral HPLC and
9
10 then both enantiomers were separated by chiral prep. HPLC: (Chiralpak AD-H (250x4.6) mm, 5 μ m; n-
11
12 hexane/IPA = 60:40). The first peak eluted at Rt 7.35 min (6.5 g) and the second at Rt 10.0 min (5 g).

13
14 Deconvolution of the enantiomers revealed in retro perspective that the later eluting peak was the desired
15
16 R enantiomer. ^1H NMR (400 MHz, DMSO- d_6) δ 7.68-7.65 (m, 2H), 7.43-7.39 (m, 2H), 7.21-7.17 (m, 1H), 6.55
17
18 (s, 1H), 4.20-4.10 (m, 2H), 3.89-3.83 (m, 2H), 2.50-2.48 (m, 1H), 2.52-2.13 (m, 1H), 1.18 (t, J = 7.12 Hz, 3H).
19
20 LCMS: (Method A) 250.3 (M+H), Rt. 2.96 min, 99.11 % (Max). HPLC: Rt 3.04 min, 98.34 % (Max), 97.20 %
21
22 (254 nm). Chiral HPLC (crude): (Method A) Rt (min): 7.35 min and 10.00 min, area % 49.55/50.45. Chiral
23
24 HPLC (after prep): (Method B) Rt 11.65 min, area 99.7%.

25 26 27 **(R)-3-hydroxy-2-oxo-1-phenyl-pyrrolidine-3-carboxylic acid (16)**

28
29 To a solution of (R)-3-hydroxy-2-oxo-1-phenyl-pyrrolidine-3-carboxylic acid ethyl ester (*R*-**15**, 3.5g,
30
31 14.05mmol) in THF:H₂O (3:1) was added LiOH.H₂O (2.36 g, 56.19 mmol) and stirred for 4 h. After
32
33 completion of the reaction, the solvent was removed by vacuum and acidified with HCl (1.5N). The
34
35 aqueous solution was extracted with ethyl acetate and dried over sodium sulphate. The solvent was
36
37 evaporated under vacuum to afford the title compound in 84 % yield (2.6g, brown solid). ^1H NMR (400
38
39 MHz, DMSO- d_6) δ 7.69-7.66 (m, 2H), 7.42-7.37 (m, 2H), 7.20-7.16 (m, 1H), 3.86-3.82 (m, 2H), 2.56-2.53
40
41 (m, 1H), 2.15-2.08 (m, 1H). LCMS: (Method A) 222 (M+H), Rt. 2.07 min, 98.67 (max); 98.71 (254nm).
42
43 HPLC: Rt 2.16 min, 98.66 (max); 98.89 (254nm). Chiral HPLC (after prep): (Method C) Rt 12.10 min, area
44
45 % 100.

46 47 48 **Synthesis of building block R-18**

49 50 *Synthesis of 2-Oxo-pyrrolidine-1-carboxylic acid tert-butyl ester*

51
52 To a solution of 2-pyrrolidinone **17** (60g, 368mmol) in dry acetonitrile (600ml) was added DMAP (4.39g,
53
54 36.8mmol). Then BOC₂O (200g, 460mmol) was added slowly at 0°C. The reaction was slowly warmed to
55
56 rt and stirred for additional 3h under nitrogen. After completion of the reaction, the solvent was
57
58
59
60

1
2
3
4
5
6 removed completely under reduced pressure and the crude was suspended with water, extracted with
7
8 ethyl acetate and washed with 1.5N HCl solution. The organic layer was separated, dried over NaSO₄ and
9
10 concentrated under reduced pressure. The obtained brown liquid was purified by column
11
12 chromatography (60-120 mesh) with 30% ethyl acetate in petrol ether to afford 92 g (70%) of the title
13
14 compound as a pale yellow liquid. ¹H NMR (400 MHz, DMSO-d₆): δ 3.64-3.60 (m, 2H), 2.40-2.36 (m, 2H),
15
16 1.91-1.83 (m, 2H), 1.43 (s, 9H).
17

18
19 *Synthesis of 2-Oxo-pyrrolidine-1,3-dicarboxylic acid 3-benzyl ester 1-tert-butyl ester*

20
21 To a solution of 2-Oxo-pyrrolidine-1-carboxylic acid tert-butyl ester (50g, 270mmol) in dry THF (500ml)
22
23 was added LiHMDS (1M in THF; 540 ml, 540 mmol) at -78°C under nitrogen slowly. After the addition was
24
25 completed, stirring was continued at -78°C for another hour. Then benzyl chloroformate (50% solution in
26
27 toluene; 90 ml, 270 mmol) was added dropwise at -78°C under nitrogen. The reaction mass was slowly
28
29 warmed to rt and stirred for 1h at that temperature. The reaction was quenched with ice and extracted
30
31 with ethyl acetate. The organic layer was washed with 10% NaHCO₃ and brine. The organic layer was
32
33 separated, dried over Na₂SO₄ and was concentrated under reduced pressure. The crude obtained was
34
35 made into a slurry with petrol ether and the obtained solid was filtered through vacuum. The yellow
36
37 crude was further purified by column chromatography (60-120 mesh) with 40% ethyl acetate in petrol
38
39 ether to afford 37 g (43 %) of the title compound as an off white solid. ¹H NMR (400 MHz, DMSO-d₆): δ
40
41 7.38-7.33 (m, 5H), 5.20-5.13 (m, 2H), 3.80-3.69 (m, 2H), 3.62-3.55 (m, 1H), 2.24-2.14 (m, 2H), 1.44 (s, 9H).
42
43
44

45
46 *Synthesis of 2-Oxo-pyrrolidine-1,3-dicarboxylic acid 1-tert-butyl ester*

47
48 To a solution of 2-Oxo-pyrrolidine-1,3-dicarboxylic acid 3-benzyl ester 1-tert-butyl ester (37g, 116mmol)
49
50 in dry methanol (400 ml) was added Pd/C (10 %; 3.7g) and the suspension was stirred at rt under
51
52 hydrogen atmosphere. The reaction mass was filtered through celite. The filtrate was evaporated under
53
54 reduced pressure to afford 24 g (90%) of the title compound as a white solid. ¹H NMR (400 MHz, DMSO-
55
56 d₆): δ 12.94 (s, 1H), 3.72-3.66 (m, 1H), 3.62-3.50 (m, 2H), 2.23-2.18 (m, 2H), 1.44 (s, 9H).
57

58
59 *Synthesis of 3-(3-Chloro-5-fluoro-benzylcarbamoyl)-2-oxo-pyrrolidine-1-carboxylic acid tert-butyl ester*
60

1
2
3
4
5
6 To a solution of 2-Oxo-pyrrolidine-1,3-dicarboxylic acid 1-tert-butyl ester (6 g; 26 mmol) and 3-chloro-5-
7 fluoro benzyl amine (5 g; 31.4 mmol) in dry DCE (60 ml) was added TEA (11 ml) and T3P (25 ml; 78 mmol)
8 under ice cooled condition. The reaction was stirred at rt for 1h under nitrogen. After the reaction was
9 completed, it was diluted with DCE and washed with 10% NaHCO₃ and brine. The organic layer was
10 separated, dried over Na₂SO₄ and concentrated under reduced pressure. The obtained crude was
11 purified by column chromatography (60-120mesh) 40 % ethyl acetate in petrol ether giving the product
12 in 87 % yield (8.4 g) as colorless solid. ¹H NMR (400 MHz, DMSO-d₆): δ 8.92-8.03 (m, 1H), 7.31-7.28 (m,
13 1H), 7.23 (s, 1H), 7.14-7.12 (m, 1H), 4.44-4.39 (m, 1H), 4.27-4.22 (m, 1H), 3.73-3.52 (m, 3H), 2.17-2.10 (m,
14 2H), 1.45 (s, 9H).

25 *Synthesis of 2-Oxo-pyrrolidine-3-carboxylic acid 3-chloro-5-fluoro-benzylamide*

26
27 To a solution of 3-(3-Chloro-5-fluoro-benzylcarbamoyl)-2-oxo-pyrrolidine-1-carboxylic acid tert-butyl
28 ester (8.4 g, 22.7 mmol) in dry 1,4-dioxane (70 ml) was added a saturated solution of HCl in dioxane (100
29 ml) under ice cooled condition. The reaction was warmed slowly to rt and stirred for additional 2 h under
30 nitrogen. After completion of the reaction, the liquid phase was concentrated to dryness under reduced
31 pressure. The obtained solid was washed with petrol ether and dried over Na₂SO₄ to afford 6 g (86 %) of
32 the title compound as a white solid. ¹H NMR (400 MHz, DMSO-d₆): δ 8.62-8.60 (m, 1H), 7.86 (s, 1H), 7.28-
33 7.25 (m, 2H), 7.17-7.14 (m, 1H), 4.46-4.41 (m, 1H), 4.24-4.19 (m, 1H), 3.25-3.18 (m, 2H), 2.32-2.27 (m,
34 1H), 2.18-2.14 (m, 1H).

45 *Synthesis of 3-Hydroxy-2-oxo-pyrrolidine-3-carboxylic acid 3-chloro-5-fluoro-benzylamide (18)*

46
47 To a solution of 2-Oxo-pyrrolidine-3-carboxylic acid 3-chloro-5-fluoro-benzylamide (6 g, 19 mmol) in dry
48 tert-butanol (60 ml) was added sodium ethoxide (20% in ethanol; 20 ml, 58 mmol) and tert-butyl hydro
49 peroxide (70% aq. solution; 7.7 ml, 58 mmol) slowly under ice cooled condition. After the addition was
50 completed, the reaction was refluxed at 75^oC for 1h. The reaction was evaporated to dryness under
51 reduced pressure. The obtained crude was diluted with water and extracted with ethyl acetate. The
52 combined organic layer was dried over sodium sulphate and concentrated under reduced pressure. The
53
54
55
56
57
58
59
60

1
2
3
4
5
6 obtained pale yellow solid was washed with DCE to afford 2.7 g (48 %) of the title compound as a white
7
8 solid which was confirmed as racemic mixture by chiral HPLC analysis. LCMS: Mass found ($M+H^+$, 287.0).
9
10 Method A: Rt 2.69 min, area % 97.74 (max), 97.48 (220nm) HPLC: Rt 2.71 min, area % 99.12 (max), 9.06
11
12 (220 nm).
13

14 The racemate was separated into the enantiomers via chiral chromatography giving the 1.3 g of the
15
16 desired *R*-**18**. Chiral HPLC: Chiralcel OJ-H (250 X 4.6) mm, 5 μ m, Mobile Phase: 0.1% DEA in hexane/IPA =
17
18 90:10, flow:1.0 mL/min, Rt 13.23 min. 1H NMR (400 MHz, DMSO- d_6): δ 8.55 (t, J = 6.40 Hz, 1H), 7.99 (s,
19
20 1H), 7.27-7.24 (m, 1H), 7.20 (s, 1H), 7.11-7.08 (m, 1H), 6.38 (s, 1H), 4.39-4.34 (m, 1H), 4.24-4.18 (m, 1H),
21
22 3.23-3.20 (m, 2H), 2.51-2.45 (m, 1H), 2.02-1.97 (m, 1H); HRMS calcd for $C_{12}H_{13}ClFN_2O_3$ ($M+H^+$) 287.0593
23
24 found 287.0603.
25
26

27 (3*S*)-*N*-[(3-chloro-5-fluorophenyl)methyl]-3-hydroxy-1-methyl-2-oxopyrrolidine-3-carboxamide (**19**)

28
29
30 *Synthesis of 1-Methyl-2-oxo-pyrrolidine-3-carboxylic acid ethyl ester*

31
32 To a solution of *N*-methyl pyrrolidone (5 g, 50 mmol) in dry THF (50 ml) was added lithium bis-trimethyl
33
34 silyl amide (1 M in THF, 100 mL, 100 mmol) slowly at $-78^\circ C$ under nitrogen. After addition was
35
36 completed, stirring was continued at $-78^\circ C$ for another 1h. Then ethyl chloroformate (5.73 mL, 60 mmol)
37
38 was added dropwise at $-78^\circ C$ under nitrogen. The reaction mass slowly warmed to rt and was stirred for
39
40 1h. The reaction was quenched with ice and extracted with ethyl acetate. The organic layer was washed
41
42 with 10% sodium bicarbonate and brine. The organic layer was dried over sodium sulphate and
43
44 concentrated under reduced pressure to afford the title compound as a brown liquid in 48 % yield (4.1
45
46 g). LCMS: (Method A) 172.2 ($M+H^+$); Rt 0.98 min, 91.54 (max).
47
48

49
50 *Synthesis of 1-Methyl-2-oxo-pyrrolidine-3-carboxylic acid*

51
52 To a solution of 1-Methyl-2-oxo-pyrrolidine-3-carboxylic acid ethyl ester (1.6 g, 9.35 mmol) in THF: H_2O
53
54 (3:1) was added LiOH. H_2O (1.57 g, 37.4 mmol) and the mixture was stirred for 4 h. After completion of
55
56 the reaction, the solvent was removed by vacuum and acidified with 1.5 N HCl. The aqueous solution was
57
58 extracted with ethyl acetate and dried over sodium sulphate. The solvent was evaporated under vacuum
59
60

1
2
3
4
5
6 to afford the title compound as a brown solid in 30 % yield (400 mg). LCMS: (Method C) 144.2 (M+H), Rt.
7
8 0.83 min, 90.22 %.

9
10 *Synthesis of 1-Methyl-2-oxo-pyrrolidine-3-carboxylic acid 3-chloro-5-fluoro-benzylamide*

11
12 To a solution of 1-Methyl-2-oxo-pyrrolidine-3-carboxylic acid (400 mg, 2.79 mmol) and 3-chloro-5-fluoro
13
14 benzyl amine (0.448 mg, 2.79 mmol) in dry DCE (60 mL) was added TEA (1.16 mL, 8.39 mmol) and T3P
15
16 (2.67 g, 8.39 mmol) under ice cooled condition. The reaction mass was stirred at rt for 1h under nitrogen.
17
18 The reaction was diluted with DCE and extracted with 10% NaHCO₃ and brine. The organic layer was
19
20 dried over Na₂SO₄ and concentrated under reduced pressure. The crude obtained was purified by column
21
22 chromatography (60-120mesh). The product was eluted with 50 % ethyl acetate in petrol ether to afford
23
24 the title compound in 51 % yield (400 mg). ¹H NMR (400 MHz, DMSO-d₆) δ 8.66 (t, J = 6.9 Hz, 1H), 7.29-
25
26 7.24 (m, 2H), 7.17-7.14 (m, 1H), 4.46-4.24 (m, 1H), 4.23-4.19 (m, 1H), 3.34-3.29 (m, 3H), 2.74 (s, 3H),
27
28 2.22-2.19 (m, 1H), 2.13-2.10 (m, 1H).

29
30
31 **(S)-N-[(3-chloro-5-fluorophenyl)methyl]-3-hydroxy-1-methyl-2-oxopyrrolidine-3-carboxamide (19)**

32
33 To a solution of 1-Methyl-2-oxo-pyrrolidine-3-carboxylic acid 3-chloro-5-fluoro-benzylamide (400 mg, 1.4
34
35 mmol) in dry tert-butanol (10 mL) was added sodium ethoxide (20% in ethanol; 1.9 mL, 5.6 mmol) and
36
37 tert-butyl hydro peroxide (70 % aq. solution; 0.72 mL, 5.6 mmol) slowly under ice cooled condition. After
38
39 the addition was completed, the reaction mass was refluxed at 75°C for 1h. The reaction mass was
40
41 evaporated completely under reduced pressure. The obtained residue was diluted with water and
42
43 extracted with ethyl acetate (5 times). The combined organic layer was dried over Na₂SO₄ and
44
45 concentrated under reduced pressure. The obtained pale yellow solid was washed with DCE to afford the
46
47 title compound as a white solid which was found to be a racemic mixture as analyzed by chiral HPLC and
48
49 was then separated by chiral prep. HPLC to afford the required isomer in 39% yield (69 mg) as off white
50
51 solid. ¹H NMR (400 MHz, DMSO) δ 8.59 (t, J = 6.4, 1H), 7.31 – 7.23 (m, 1H), 7.19 (s, 1H), 7.09 (d, J = 9.8,
52
53 1H), 6.46 (s, 1H), 4.36 (dd, J = 15.7, 6.8, 1H), 4.21 (dd, J = 15.8, 5.8, 1H), 2.76 (s, 3H), 2.45 – 2.40 (m, 1H),
54
55
56
57
58
59
60

2.00 – 1.88 (m, 1H). LCMS: (Method A) 301 (M+H), Rt. 2.93 min, 98.94 (max), 99.00 (254nm). HPLC: Rt 2.86 min, 96.37 (max), 96.56 (254nm); HRMS calcd for C₁₃H₁₅ClFN₂O₃ (M+H⁺) 301.075 found 301.0756.

(S)-3-Hydroxy-2-oxo-1-(2-oxo-2,3-dihydro-1H-indol-5-yl)-pyrrolidine-3-carboxylic acid 3-chloro-5-fluorobenzylamide (**20**)

The title compound was prepared as described for compounds **11ra** – **11rj** in 30% yield (33.4 mg). Rt 6.16 min. ¹H NMR (400 MHz, DMSO-d₆) δ 10.36 (s, 1H), 8.66 (t, J = 6.4 Hz, 1H), 7.56 (d, J = 2.1 Hz, 1H), 7.41 (dd, J = 8.5, 2.2 Hz, 1H), 7.26 (dt, J = 8.8, 2.2 Hz, 1H), 7.21 (d, J = 1.7 Hz, 1H), 7.10 (ddd, J = 9.7, 2.4, 1.4 Hz, 1H), 6.83 (d, J = 8.4 Hz, 1H), 6.68 (s, 1H), 4.39 (dd, J = 15.8, 6.7 Hz, 1H), 4.25 (dd, J = 15.7, 6.0 Hz, 1H), 3.80 (dd, J = 7.7, 5.9 Hz, 2H), 3.50 (s, 2H), 2.58 (dt, J = 12.9, 5.8 Hz, 1H), 2.11 (dt, J = 12.9, 7.6 Hz, 1H); ¹³C NMR (176 MHz, DMSO-d₆) δ 175.70, 171.21, 170.28, 162.19, 160.79, 143.67, 143.62, 140.06, 133.06, 133.00, 132.67, 125.65, 122.48, 122.46, 118.97, 116.65, 113.56, 113.42, 112.12, 112.00, 108.26, 78.59, 44.97, 40.50, 35.42, 30.96. HRMS calcd for C₂₀H₁₈ClFN₃O₄ (M+H⁺) 418.0964 found 418.097.

(S)-3-Hydroxy-2-oxo-1-(2-oxo-1,2,3,4-tetrahydro-quinolin-6-yl)-pyrrolidine-3-carboxylic acid 3-chloro-5-fluorobenzylamide (**21**)

The title compound was prepared as described for compounds **11ra** – **11rj** in 17 % yield (35 mg). ¹H NMR (400 MHz, DMSO-d₆) δ 12.06 (s, 1H), 10.10 (s, 1H), 8.70 (t, J = 6.3, 1H), 7.65 (s, 1H), 7.47 (s, 1H), 7.43 (dd, J = 8.6, 2.4, 1H), 7.27 (dt, J = 8.7, 2.1, 1H), 7.20 (s, 1H), 7.09 (d, J = 8.9, 1H), 7.03 (s, 2H), 6.85 (d, J = 8.6, 1H), 6.72 (s, 1H), 4.37 (dd, J = 15.7, 6.8, 1H), 4.23 (dd, J = 15.7, 6.1, 1H), 3.79 (t, J = 6.8, 1H), 2.87 (t, J = 7.6, 1H), 2.61 – 2.52 (m, 1H), 2.43 (dd, J = 8.3, 6.7, 2H), 2.09 (dt, J = 12.9, 7.6, 1H). LCMS: (Method A) 432 (M+H), Rt. 3.36 min, 91.39(max), 92.24(254nm); HPLC: Rt 3.47 min, 93.70 (max), 93.73 (254nm); chiral HPLC (after prep) (Method B) Rt 9.77 min, area % 100; HRMS calcd for C₂₁H₂₀ClFN₃O₄ (M+H⁺) 432.1121 found 432.1129.

Biological assays

Biochemical activity testing of MetAP-2

1
2
3
4
5
6 MetAP-2 activity was determined by an enzyme-coupled assay using the tripeptide Met-Ala-Ser (MAS) as
7
8 substrate and recombinant human MetAP-2 (His-Tev- MetAP-2, prepared at Merck). The released
9
10 methionine is converted by L-amino acid oxidase (AAO) to oxidized Methionine and hydrogen peroxide is
11
12 released. In a second step horse radish peroxidase catalyzes the oxidation of the leuco dye dianisidine to
13
14 oxidized dianisidine using hydrogen peroxide as co-substrate. The produced dianisidine ox was detected
15
16 photometrically as increase in absorbance at 450 nm. Met-AP2 activity was determined in a kinetic
17
18 measurement mode. The release of one molecule methionine corresponds to the production of one
19
20 molecule dianisidine ox. The MetAP2 enzymatic activity is directly corresponding to the increase in
21
22 absorbance per time.
23
24

25
26 In detail, the assay was performed in 384 well microtiter plate (Greiner 78110 MTP, transparent) in a
27
28 total reaction volume of 50 μ l at 22°C. 0.35 μ g of N-terminal His tag human rec MetAP2 (prepared in
29
30 house, AA 2-478, final concentration (fc) 123 nM), 1 unit horse radish Peroxidase (Roche, Mannheim),
31
32 0.02 unit L-amino acid oxidase (Merck, Darmstadt), 0.6 mM dianisidine (Merck, Darmstadt, dissolved in
33
34 50 mM HCl, 10% DMSO) were incubated in the absence or presence of the test compound (10 dilution
35
36 concentrations) in 100 mM Hepes, 50 mM NaCl, 50 μ M MnCl₂ at pH 7.0 for 15 min at 22 °C. The reaction
37
38 was started by the addition of 500 μ M (fc) MAS peptide (Merck, Darmstadt). After mixing the first
39
40 absorbance measurement was performed on an Envision multimode reader (Perkin–Elmer, Waltham) at
41
42 wavelength of 450 nm. The reaction was incubated at 22°C for additional 45 min and the second
43
44 absorbance measurement was performed. The increase of absorbance per time was determined. The
45
46 control value used was the inhibitor- free reaction with 0.5 % DMSO (fc). As pharmacological inhibitor
47
48 control Fumagillin (Merck, Darmstadt) in a final concentration of 5 μ M was used. The inhibitory values
49
50 (IC₅₀) were determined using the program ASSAY ANALYZER® from GeneData (Basel, Switzerland).
51
52

53 **HUVEC proliferation assay**

54
55 Proliferation of HUVEC primary endothelial cells was used as cell-based mechanistical assay.²⁵ Applying
56
57 the CyQUANT® Direct Cell Proliferation Assay (Invitrogen C35011) which is based on a cell-permeant
58
59
60

1
2
3
4
5
6 fluorescent DNA-binding dye, DNA content is used as a direct measure for cell number. Pooled HUVEC
7
8 cells (Promocell C-12203) are cultivated in the medium supplied by Promocell (Cat No C-22020) for
9
10 maximum 4 passages. For the assay 500 cells/well are seeded into black 384-well culture plates with
11
12 clear bottom in 70 μ l culture medium and incubated for 6 hours at 37°C, 5 % CO₂. 10 μ l prediluted test
13
14 compounds are added and cells incubated for 3 days at 37°C, 5 % CO₂ before measurement of DNA
15
16 content. CyQUANT detection reagent is prepared according to the manufacturers protocol, 20 μ l/well
17
18 added and incubated at 37°C, 5 % CO₂ for at least 1h before measurement of fluorescence at Envision
19
20 multimode reader (Perkin–Elmer, Waltham) with excitation 480 nm and emission 535 nm (bottom read
21
22 mode). The assay is performed as dose response with 10 compound dilutions. Inhibitory values (IC₅₀)
23
24 were determined using the program ASSAY ANALYZER® from GeneData (Basel, Switzerland).
25
26

27 **Efficacy Testing *in vivo*** (all animal experiments performed in the manuscript were conducted in
28
29 compliance with institutional guidelines)

30
31
32 The human U87-MG cell line (derived from malignant glioma, ATCC: HTB-14) used was directly prepared
33
34 from frozen cell batches for tumor cell inoculation. Cell vials were rapidly thawed at 37°C. Cell suspension
35
36 of all vials was transferred into a sterile 50ml centrifuge tube (Falcon). The tube was filled with PBS (w/o
37
38 Ca/ Mg) up to 50ml, mixed and cell number and viability measured with ViCell (Automated Cell Viability
39
40 Analyzer; Beckman Coulter). Cell suspension was centrifuged for 5min at 1000g and adjusted to 10x10⁶
41
42 viable cells/ml using PBS (w/o Ca/ Mg). 100 μ l of the cell suspension were subcutaneously inoculated in
43
44 the right flank of nude mice. In the present study female CD-1 nude mice, aged 6-7 weeks, were used. CD-
45
46 1 nude mice are an outbred strain provided by Charles River Laboratories (CRL), Sulzfeld, Germany. The
47
48 mice were housed and maintained under aseptic conditions in facilities approved by the German
49
50 Association for Accreditation of Laboratory Animal Care and in accordance with current regulations and
51
52 standards of the German Animal Protection Law, and their use was approved by the local responsible
53
54 authorities.
55
56
57
58
59
60

1
2
3
4
5
6 Animal identification: All animals were individually identified using subcutaneously implanted electronic
7
8 NONATEC transponders (LUTRONIC, Luxemburg). Implantation was performed on the back by hypodermic
9
10 needle (18 gauge) after sterilization of the skin with 70% alcohol. An electronic reader allowed the
11
12 identification of each individual animal with the corresponding code number.

13
14 Formulation: 20 has been dissolved in 0,5%Methocel/ 0,25%Tween20 in Milli-Q water and stored at 4°C.

15
16 Compound solution has been freshly prepared all 3-4 days. Treatment: On treatment days the solution
17
18 was allowed to return to room temperature followed by per os administration of 200 µl per 20g mouse.

19
20 Tumor volume and body weight measurements and calculations: When the tumors had reached a mean
21
22 tumor volume typically of 300-400 mm³, the animals were assigned to treatment groups (8 or 10
23
24 animals/group). Tumor length (L) and width (W) were measured twice weekly by calipers. The tumor
25
26 volume was calculated using the formula $L \times W^2 / 2$. Body weight was monitored twice weekly. All animal
27
28 data were collected in an electronical data collection system. T/C-value: The effect of a treatment on
29
30 tumor growth was assessed at the end of each study by calculating the % T/C value according to
31
32 following formulas: % T/C (for mean values > 0): [(end tumor volume treatment - start tumor volume
33
34 treatment)/(end tumor volume control - start tumor volume control)] x 100]

35 36 37 38 **Supporting Information**

39
40 X-ray structure generation, additional graphics superimposition of **11a** with methionine and individual
41
42 tumor volumes from *in vivo* experiment.

43 44 45 **PDB cods:**

46
47 **1** (SB-587094): 2OAZ; **2** (A-357300): 1R58; **3** (LAF-153): 1QZY; **4**: 5JFR; **5** (A-849519): 1YW9; **6**: 5LYX7 (JNJ-
48
49 4929821): 6QEJ; **8** (GSK-2229238): 6QEI; **9** (X = Cl; Clioquinol): 6QEH; **11a**: 6QEG; 11r: 6QEF; **21**: 6QED.

50
51 Authors will release the atomic coordinates and experimental data upon article publication.

52 53 **Author information**

54
55 Timo Heinrich, timo.heinrich@merckgroup.com, Tel.: +49 61 51 72 65 89

56 57 58 **Abbreviations used**

1
2
3
4
5
6 Meldrum's acid, 6,6-dimethyl-5,7-dioxaspiro[2.5]octane-4,8-dione; NMR, nuclear magnetic resonance;
7
8 HPLC, high-performance liquid chromatography; HUVEC, human umbilical vein endothelial cells; vdW,
9
10 van der Waals; EDCI, N-(3-Dimethylaminopropyl)-N'-ethylcarbodiimid hydrochloride ; HOBt, 1-
11
12 Hydroxybenzotriazol hydrate ; MMPP, Magnesium monoperoxyphthalat; pKa; logarithmic acid
13
14 dissociation constant; T/C, ratio of tumor size for treatment (T) and control (C) group; T3P;
15
16 propylphosphonic anhydride; BOC₂O, di-tert-butyl decarbonate; Rt, retention time; TEA, triethyl amine;
17
18 IPA, isopropylamine; LiHMDS, lithium bis-trimethyl silyl amide.
19
20

21 **References and Notes**

22
23
24 ¹ Yin, S.-Q.; Wang J.-J., Zhang, C.-M.; Liu, Z.-P. The development of MetAP-2 inhibitors in cancer
25
26 treatment. *Curr. Med. Chem.* **2012**, *19*, 1021-1035.

27
28
29 ² Ehlers, T.; Furness, S.; Robinson, T. P.; Zong, H. A.; Goldsmith, D.; Aribser, J.; Bowen, J. P. Methionine
30
31 aminopeptidase type-2 inhibitors targeting angiogenesis. *Curr. Top. Med. Chem.* **2016**, *16*, 1478-1488.

32
33
34 ³ McCandless, S. E.; Yanovski, J. A.; Miller, J.; Fu, C.; Bird, L. M.; Salehi, P.; Chan, C. L.; Stafford, D.;
35
36 Abuzzahab, M. J.; Viskochil, D. Effects of MetAP-2 inhibition on hyperphagia and body weight in Prader-
37
38 Willi syndrome: A randomized, double-blind, placebo-controlled trial. *Diabetes, Obesity and Metabolism*
39
40 **2017**, *19*, 1751-1761.

41
42 ⁴ Kudelka, A.P.; Levy, T.; Verschraegen, C.F.; Edwards, C.L.; Piamsomboon, S.; Termrungruanglert, W.;
43
44 Freedman, R.S.; Kaplan, A.L.; Kieback, D.G.; Meyers, C.A.; Jaeckle, K.A.; Loyer, E.; Steger, M.; Mante, R.;
45
46 Zavligit, G.; Killian, A.; Tang, R.A.; Gutterman, J.U.; Kavanagh, J.J. A phase I study of TNP-470
47
48 administered to patients with advanced squamous cell cancer of the cervix. *Clin. Cancer Res.* **1997**, *9*,
49
50 1501-1505.

51
52
53 ⁵ Kruger, E. A.; Figg, F. D. TNP-470: an angiogenesis inhibitor in clinical development for cancer. *Expert*
54
55 *Opin. Investig. Drugs* **2000**, *6*, 1383-1396.
56
57
58
59
60

- 1
2
3
4
5
6
-
- 7 ⁶ Wang, J.; Sheppard, G., S.; Lou, P.; Kawai, M.; Park, C.; David A. Egan, D.A.; Schneider, A.; Bouska, J.;
8
9 Lesniewski, R.; Henkin, J. Physiologically relevant metal cofactor for methionine aminopeptidase-2 is
10 manganese. *Biochemistry* **2003**, *42*, 5035-5042.
- 11
12
13 ⁷ Joseph P. Marino, Jr., Paul W. Fisher, Glenn A. Hofmann, Robert B. Kirkpatrick, Cheryl A. Janson, Randall
14
15 K. Johnson, Chun Ma, Michael Mattern, Thomas D. Meek, M. Dominic Ryan, Christina Schulz, Ward W.
16
17 Smith, David G. Tew, Thaddeus A. Tomazek, Jr., Daniel F. Veber, Wenfang C. Xiong, Yuuichi Yamamoto,
18
19 Keizo Yamashita, Guang Yang, and Scott K. Thompson Highly potent inhibitors of methionine
20
21 aminopeptidase-2 based on a 1,2,4-triazole pharmacophore. *J. Med. Chem.* **2007**, *50*, 3777-3785.
- 22
23
24 ⁸ Burley, S.K.; David, P.R.; Lipscomb, W.N. Leucine aminopeptidase: bestatin inhibition and a model for
25
26 enzyme-catalyzed peptide hydrolysis. *Proc. Natl. Acad. Sci. USA*, **1991**, *88*, 6916–6920.
- 27
28
29 ⁹ Sheppard, G. S.; Wang, J.; Kawai, M.; BaMaung, N. Y.; Craig, R. A.; Erickson, S. A.; Lynch, L.; Patel, J.;
30
31 Yang, F.; Searle, X. B.; Lou, P.; Park, C.; Kim, K. H.; Henkin, J.; Lesniewski, R. 3-Amino-2-hydroxyamides
32
33 and related compounds as inhibitors of methionine aminopeptidase-2. *Bioorg. Med. Chem. Lett.* **2004**,
34
35 *14*, 865–868.
- 36
37
38 ¹⁰ Towbin, H.; Bair, K. W.; DeCaprio, J. A.; Eck, M. J.; Kim, S.; Kinder, F. R.; Morollo, A.; Mueller, D. R.;
39
40 Schindler, P.; Song, H. K.; van Oostrum, J.; Versace, R. W.; Voshol, H.; Wood, J.; Zabludoff, S.; Phillips, P.
41
42 E. Bengamides as a new class of methionine aminopeptidase inhibitors. *J. Biol. Chem.* **2003**, *278*, 52964–
43
44 52971.
- 45
46
47 ¹¹ Xu, W.; Lu, J.-P.; Qi-Zhuang, Y. Structural analysis of bengamide derivatives as inhibitors of methionine
48
49 aminopeptidases. *J. Med. Chem.* **2012**, 8021 – 8027.
- 50
51
52 ¹² White, K. N.; Tenney, K.; Crews, P. The bengamides: A mini-review of natural sources, analogues,
53
54 biological properties, biosynthetic origins, and future prospects. *J. Nat. Prod.* **2017**, *80*, 740-755.
- 55
56
57 ¹³ McBride, C.; Cheruvallath, Z.; Komandla, M.; Tang, M.; Farrell, P.; Lawson, J. D.; Vanderpool, D.; Wu, Y.;
58
59 Dougan, D. R.; Plonowski, A.; Holub, C.; Larson, C. Discovery of potent, reversible MetAP-2 inhibitors via
60

1
2
3
4
5
6
7 fragment-based drug discovery and structure-based drug design—Part 2. *Bioorg. Med. Chem. Lett.* **2016**,
8
9 *26*, 2779–2783.

10
11 ¹⁴ Sheppard, G. S.; Wang, J.; Kawai, M.; Fidanze, S. D.; BaMaung, N. Y.; Erickson, S. A.; Barnes, D. M.;
12
13 Tedrow, J. S.; Kolaczowski, L.; Vasudevan, A.; Park, D. C.; Wang, G. T.; Sanders, W. J.; Mantei, R. A.;
14
15 Palazzo, F.; Tucker-Garcia, L.; Lou, P.; Zhang, Q.; Park, C. H.; Kim, K. H.; Petros, A.; Olejniczak, E.;
16
17 Nettlesheim, D.; Hajduk, P.; Henkin, J.; Lesniewski, R.; Davidsen, S. K.; Bell, R. L. Discovery and
18
19 optimization of anthranilic acid sulfonamides as inhibitors of methionine aminopeptidase-2: A structural
20
21 basis for the reduction of albumin binding. *J. Med. Chem.* **2006**, *49*, 3832–3849.

22
23
24 ¹⁵ Heinrich, T.; Buchstaller, H.-P.; Cezanne, B.; Rohdich, F.; Bomke, J.; Friese-Hamim, M.; Krier, M.;
25
26 Knochel, T.; Musil, D.; Leuthner, B.; Zenke, F. Novel reversible methionine aminopeptidase-2 (MetAP-2)
27
28 inhibitors based on purine and related bicyclic templates. *Bioorg. Med. Chem. Lett.* **2017**, *27*, 551–556.

29
30
31 ¹⁶ Garrabrant, T.; Tuman, R. W.; Ludovici, D.; Tominovich, R.; Simoneaux, R. L.; Galemno, R. A. Jr.;
32
33 Johnson, D. L. Small molecule inhibitors of methionine aminopeptidase type 2 (MetAP-2) fail to inhibit
34
35 endothelial cell proliferation or formation of microvessels from rat aortic rings in vitro. *Angiogenesis*
36
37 **2004**, *7*, 91–96.

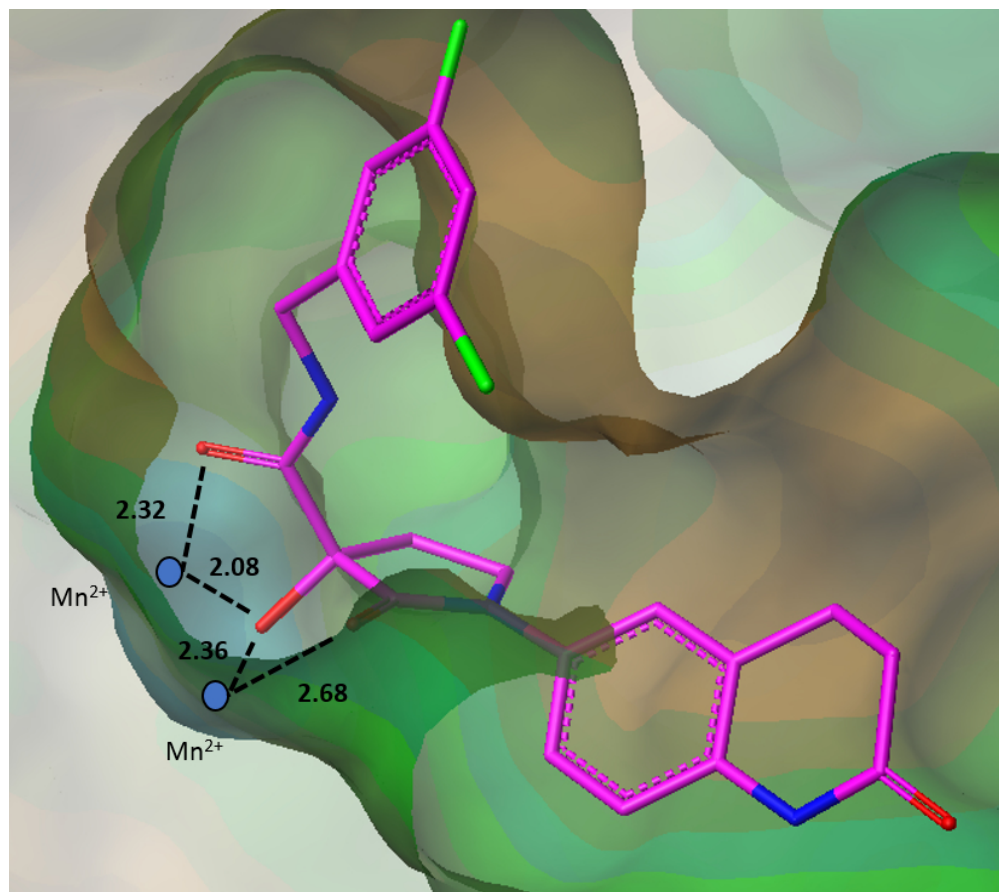
38
39
40 ¹⁷ Cowley, P.; Hales, N.; Ward, S. Highlights from the society for medicines research symposium held on
41
42 December 9, 2010 at Nhli, London UK. *Drugs of the Future*, **2011**, *36*, 543–549.

43
44
45 ¹⁸ Naber, K. G.; Niggemann, H.; Stein, G.; Stein, G. Review of the literature and individual patients' data
46
47 meta-analysis on efficacy and tolerance of nitroxoline in the treatment of uncomplicated urinary tract
48
49 infections. *BMC Infectious Diseases* **2014**, *14*, 628/1–31.

50
51
52 ¹⁹ Shim, J. S.; Matsui, Y.; Bhat, S.; Nacev, B. A.; Xu, J.; Bhang, H-e. C.; Dhara, S.; Han, K. C.; Chong, C. R.;
53
54 Pomper, M. G.; So, A.; Liu, J. O. Effect of nitroxoline on angiogenesis and growth of human bladder
55
56 cancer. *J. Natl. Cancer Inst.* **2010**, *102*, 1855–1873.

57
58
59 ²⁰ Zhang, Q.; Wang, S.; Yang, D.; Pan, K.; Li, L.; Yuan, S. Preclinical pharmacodynamic evaluation of
60
antibiotic nitroxoline for anticancer drug repurposing. *Onc. Lett.* **2016**, *11*, 3265–3272.

- 1
2
3
4
5
6
7 ²¹ Study of APL-1202 in non-muscle invasive bladder cancer patients who are resistant to one induction
8
9 course of BCG treatment (NMIBC); NCT03672240.
- 10
11 ²² Wang J.; Lou P.; Henkin J. Selective inhibition of endothelial cell proliferation by fumagillin is not due to
12
13 differential expression of methionine aminopeptidases. *J. Cell. Biochem.* **2000**, *77*, 465–473
- 14
15 ²³ We investigated the general chelation potential of the ligand and could prove that in solution none of
16
17 the metal ions which are discussed to be putative MetAP-2 co-factors is bound to the oxygen-triade. The
18
19 results will be published in a separated paper.
- 20
21
22 ²⁴ Liu, S.; Widom, J.; Kemp, C. W.; Crews, C. M.; Clardy, J. Structure of human methionine
23
24 aminopeptidase-2 complexed with fumagillin. *Science* **1998**, *282*, 1324-1327.
- 25
26 ²⁵ Asymmetric synthesis of the clinical compound M8891 was optimized and will be reported in due
27
28 course.
- 29
30
31 ²⁶ Eberhardt, E. S.; Raines, R. T. Amide-amide and amide-water hydrogen bonds: Implications for protein
32
33 folding and stability. *J. Am. Chem. Soc.* **1994**, *116*, 2149–2150.
- 34
35 ²⁷ Schönherr, D.; Wollatz, U.; Haznar-Garbacz, D.; Hanke, U.; Box, K. J.; Taylor, R.; Ruiz, R.; Beato, S.;
36
37 Becker, D.; Weitschies, W. Characterisation of selective active agents regarding pKa values, solubility
38
39 concentrations and pH profiles by SiriusT3. *Eur. J. Pharm. Biopharm* **2015**, *92*, 155-170.
- 40
41
42 ²⁸ Gulyaeva, N.; Zaslavsky, A.; Lechner, P.; Chlenov, M.; Chait, A.; Zaslavsky, B. Relative hydrophobicity and
43
44 lipophilicity of β -blockers and related compounds as measured by aqueous two-phase partitioning,
45
46 octanol–buffer partitioning, and HPLC. *Eur. J. Pharm. Science* **2002**, *17*, 81-93.
- 47
48
49 ²⁹ Ingber D.; Fujita, T.; Kishimoto, S.; Sudo, K.; Kanamaru, T.; Brem, H.; Folkman, J. Synthetic analogues of
50
51 fumagillin that inhibit angiogenesis and suppress tumour growth. *Nature* **1990**, *348*, 555-557.
- 52
53 ³⁰ Sin, N.; Meng, L.; Wang, M. Q. W.; Wen, J. J.; Bornmann, W. G.; Crews, C. M. The anti-angiogenic agent
54
55 fumagillin covalently binds and inhibits the methionine aminopeptidase, MetAP-2. *Proc. Natl. Acad. Sci.*
56
57 *USA* **1997**, *94*, 6099-6103.
- 58
59
60



Tabel of contents graphic

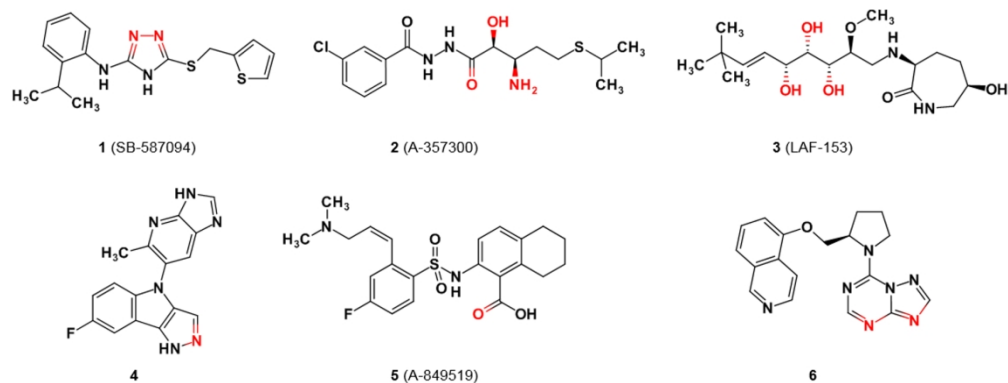


Figure 1: reversible MetAP-2 inhibitors. X-Ray structure analyses published. Metal cofactor binding atoms marked in red; PDB codes added: 1 (SB-587094) 2oaz; 2 (A-357300) 1r58; 3 (LAF-153) 1qzy; 4 5jfr; 5 (A-849519) 1yw9; 6 5lyx.

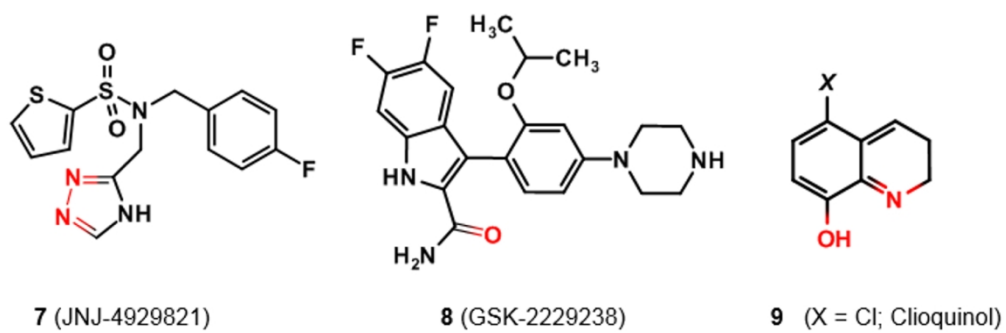
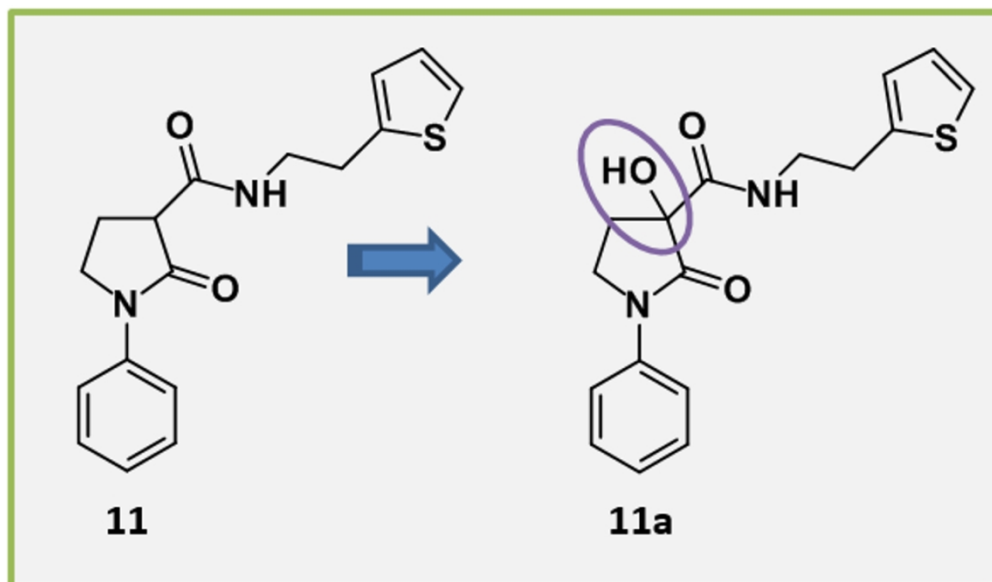


Figure 2: reversible MetAP-2 inhibitors. Synthesis and structural analyses performed in house. PDB codes added: 7 (JNJ-4929821) 6QEJ; 8 (GSK-2229238) 6QEI, 9 (X = Cl; Clioquinol) 6QEH.



26 Figure 3: The stored α -amidated pyrrolidinone **11** was oxidized to the cyclic tartronic di-amide **11a** under
27 storage in DMSO over approximately 2 years.
28
29
30
31
32
33
34
35
36
37
38
39
40
41
42
43
44
45
46
47
48
49
50
51
52
53
54
55
56
57
58
59
60

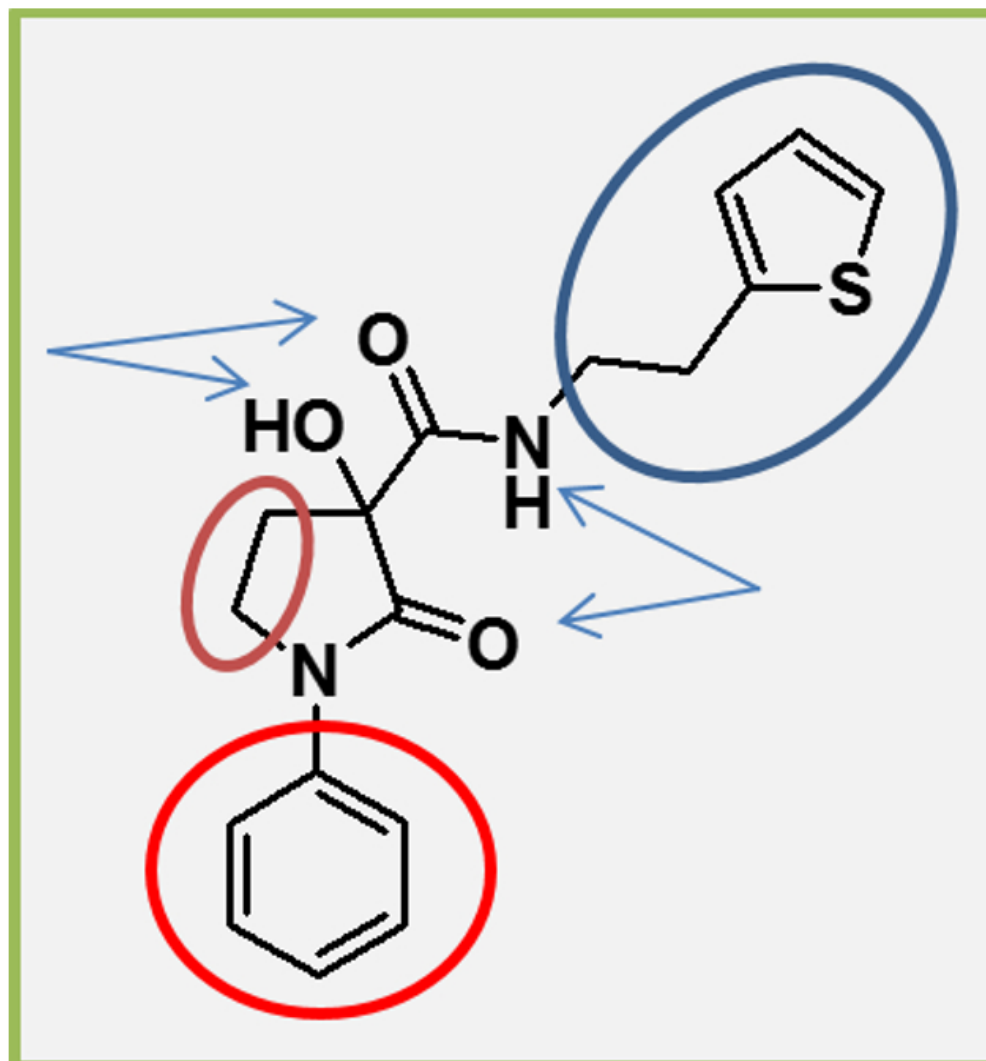


Figure 4: Screening hit rac-11a with indications of different parts of the molecule considered. The first optimization cycle focused on the amide residue highlighted by a blue circle; second improvement round considered the N-lactam residue marked with a red circle. The investigation of lactam size and additional substitutions (brown circle) as well as the heteroatoms (indicated with arrows) are not discussed here.

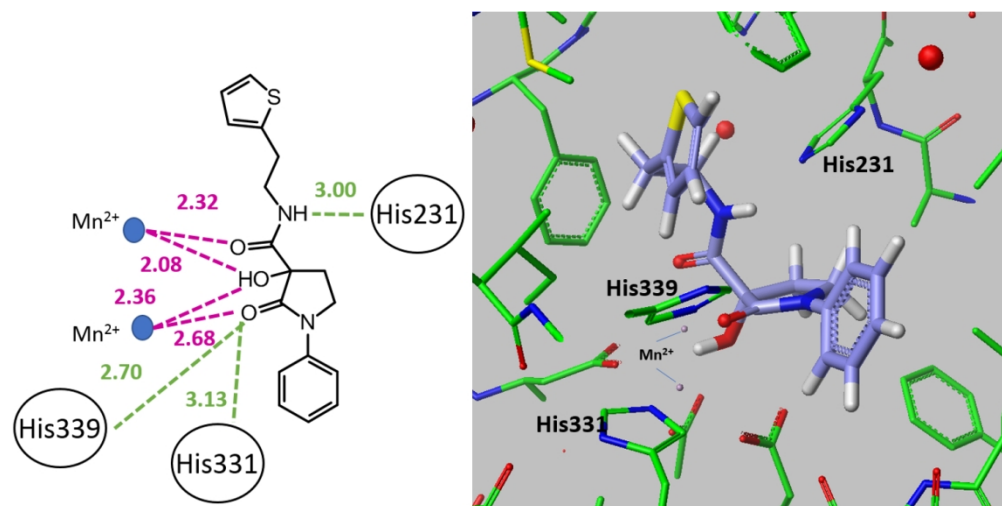


Figure 5: X-ray structure analysis of 11a in MetAP-2; A: 2D plot to show relevant polar interactions, indicated with dashed lines, oxygen-manganese contacts in purple, heteroatom-HisImidazole in green, distances are given in Ångstrom; B: Conformation of 11a in the active site; interacting imidazoles of His331 and His339 and the manganese ions are pointed out (PDB: 6QEG).

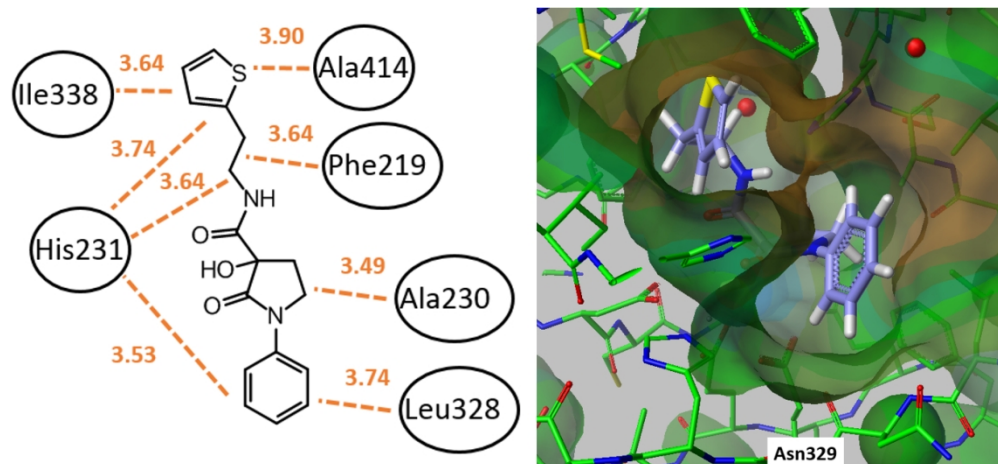


Figure 6: X-ray structure analysis of 11a in MetAP-2: A: 2D plot to show relevant lipophilic interactions, indicated with dashed lines, distances are given in Ångstrom; B: identical view on the conformation of 11a in the active site as in figure 3 B; the lipophilic trait of the protein surface is color coded. Brown indicates a lipophilic surface, green a polar one (PDB: 6QEG).

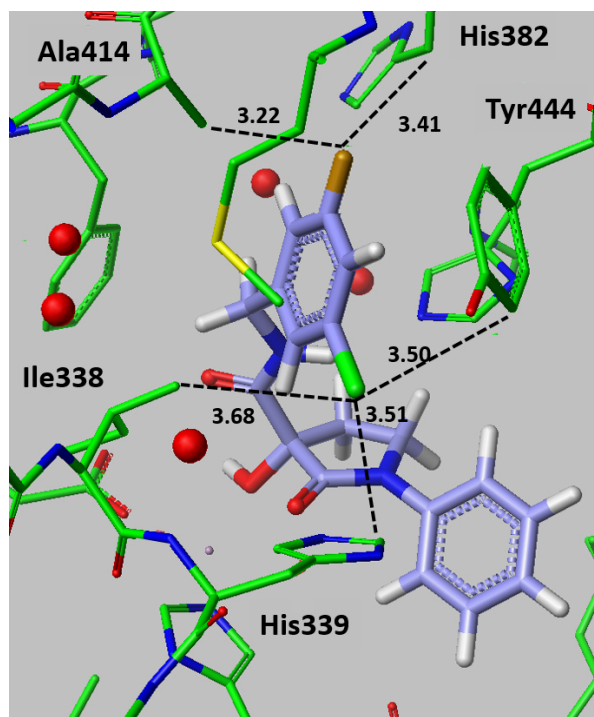


Figure 7: X-Ray structure analysis of the optimized amide residue in 11r. Depicted are only the distances of the halogens (F, top, brown; Cl, bottom, light green) on the benzamide to the amino acid side chains of MetAP-2 (6QEF).

243x172mm (120 x 120 DPI)

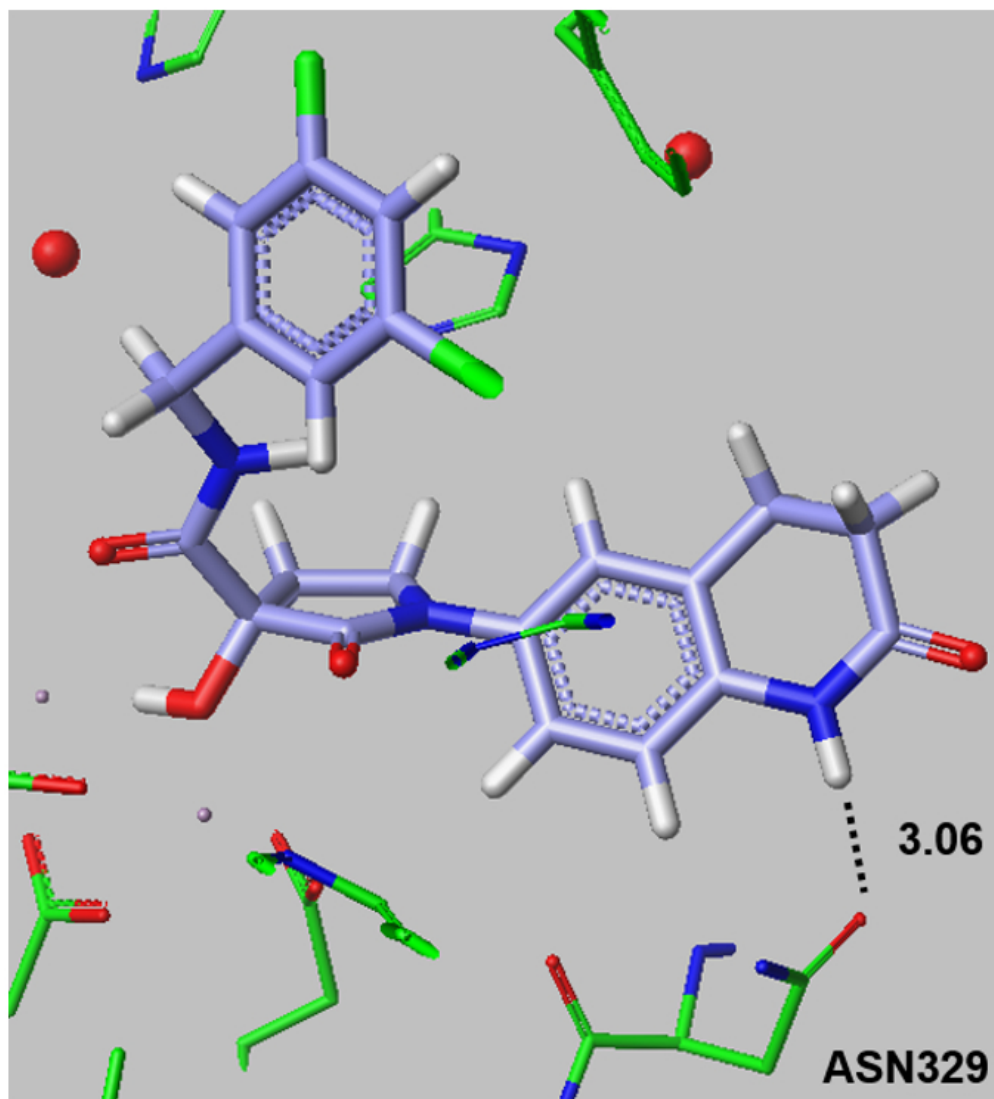


Figure 8: X-ray structure analysis of 21 with focus on the additional polar interaction of the tetrahydroquinone-NH with the ASN329 side chain amide of MetAP-2 (6QED).

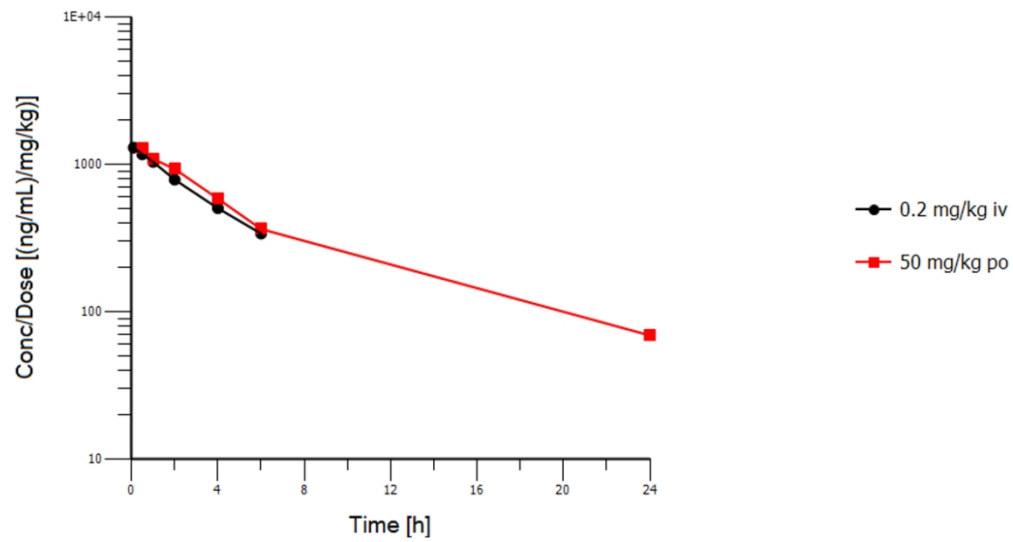
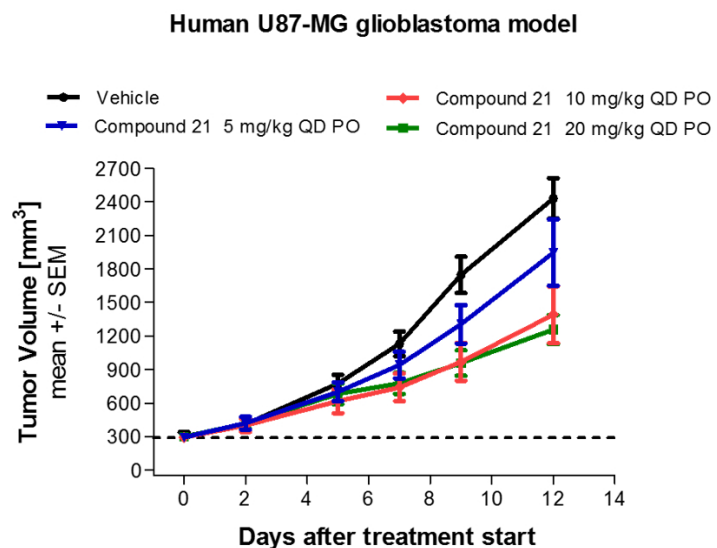
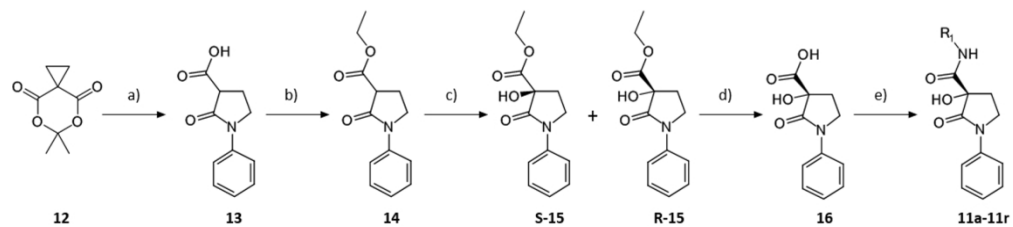


Figure 9: Dose-normalized plasma concentrations of 21 after 0.2 mg/kg iv and 50 mg/kg po dosing

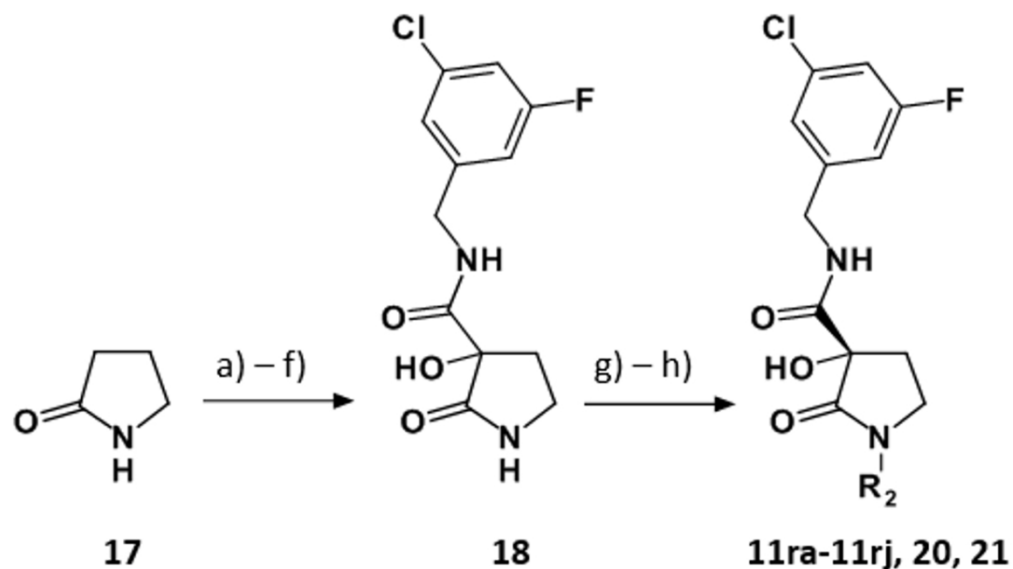


25 Figure 10: in vivo tumor growth inhibition of 21 in human U87-MG glioblastoma model. Tumor volumes for
26 the 12-day treatment period (volumes for the individual animals at the end of the study are shown in the
27 Supporting Information Figure S2).

28 243x137mm (120 x 120 DPI)



a) Reagents and conditions: a) ACN, aniline, 60°C, 12h, 85%; b) EtOH, SOCl₂, 0°C – reflux, 4h, N₂; 92% c) CeCl₃·(H₂O)₇, iPrOH, O₂, 12h, RT; Chiralpak AD-H; d) LiOH, THF/H₂O, 4h, RT; 84% e) R₁-NH₂, EDCI, HOBt, 160°C, MW, 20 min 40 – 80%.



25 a) Reagents and Conditions: a) BOC₂O, DMAP, ACN, 3h, RT, 70%; b) benzyl chloroformate, LiHMDS, THF, 2h,
26 -78°C – RT, 42%; c) Pd/charcoal, methanol, H₂, 2 bar, 2h RT, 86%; d) 3-F, 5-Cl benzylamine, T3P, TEA,
27 DCM, 5h, 0°C – RT, 86%; e) TFA, DCM, 3h, 0°C, 90%; f) MMPP, DMF, 4h, 70°C, 37%; g) R₂-halide, K₂CO₃,
28 CuI, N,N'-diethyl-ethane-1,2-diamine, dioxane, 2h, 140°C, MW; h) Chiralpak AD-H.

29
30
31
32
33
34
35
36
37
38
39
40
41
42
43
44
45
46
47
48
49
50
51
52
53
54
55
56
57
58
59
60

